Oligosaccharide production and signaling correlate with delayed flowering in an *Arabidopsis* genotype grown and selected in high [CO_2]

Short title: [CO_2] rise, carbohydrates, and flowering

Hannah Kinmonth-Schultz[1,2], Stephen Michael Walker[1], Kerem Bingol[3], David W. Hoyt[3], Young-Mo Kim[4], Lye Meng Markillie[3], Hugh D. Mitchell[4], Carrie D. Nicora[3], Ronald Taylor[4], Joy K. Ward[5]

[1]Department of Ecology and Evolutionary Biology, University of Kansas, Lawrence, KS 66045, USA [2]Departiment of Biology, Tennessee Technological University, Cookeville, TN 30585 [3]Environmental Molecular Sciences Laboratory, Pacific Northwest National Laboratory, Department of Energy, Richland, WA 99354 USA [4]Biological Sciences Division, Pacific Northwest National Laboratory, Richland, WA 99354, USA [5]College of Arts and Sciences, Department of Biology, Case Western Reserve University, Cleveland, OH 44106, USA

Author for Correspondence:

Hannah Kinmonth-Schultz

Tel: 605 828 0085

Email: hkinmonth@tntech.edu

Author Contributions:

H.K.S. Conducted much of the data analysis, data interpretation, and manuscript writing.

S.M.W. Designed and conducted the experiment, conducted early data analysis, wrote portions of the manuscript.

K.B. Contributed to experimental design for metabolite profile, conducted NMR analysis, reviewed manuscript.

D.W.H. Contributed to experimental design for metabolite profile, conducted NMR analysis, Chenomx metabolite profiling and develop metabolite workflow, contributed to manuscript.

Y-M.K. Conducted GCMS analysis, contributed to manuscript.

L.M.M. Conducted RNA sequencing and alignments to reference genomes, contributed to manuscript.

H.D.M. Conducted transcript annotations and early transcriptomic comparisons, advised on transcriptomic analyses.

C.D.N. Prepared samples for analyses, reviewed manuscript.

R.T. Conducted genome assembly, contributed to manuscript.

J.K.W. Advised on the design of the experiment and data analysis. Edited and reviewed the manuscript.

Abstract

Since industrialization began, atmospheric CO_2 ($[CO_2]$) has increased from 270 to 415 ppm and is projected to reach 800-1000 ppm this century. Some *Arabidopsis* ecotypes delayed flowering in elevated $[CO_2]$ relative to current $[CO_2]$, while others showed no change or accelerations. To predict genotype-specific flowering behaviors, we must understand the mechanisms driving flowering response to rising $[CO_2]$. $[CO_2]$ changes alter photosynthesis and carbohydrates in C_3 plants. Plants sense carbohydrate levels and exogenous carbohydrate application influences flowering time and flowering transcript levels. We asked how organismal changes in carbohydrates and transcription correlate with changes in flowering time under elevated $[CO_2]$. We used a genotype (SG) of *Arabidopsis* that was selected for high fitness at elevated $[CO_2]$ (700 ppm). SG delays flowering under elevated $[CO_2]$ (700 ppm) relative to current $[CO_2]$ (400 ppm). We compared SG to a closely related control genotype (CG) that shows no $[CO_2]$-induced flowering change. We compared metabolomic and transcriptomic profiles in these genotypes at current and elevated $[CO_2]$ to assess correlations with flowering in these conditions. While both genotypes altered carbohydrates in response to elevated $[CO_2]$, SG had higher levels of sucrose than CG and showed a stronger increase in glucose and fructose in elevated $[CO_2]$. Both genotypes demonstrated transcriptional changes, with CG increasing genes related to fructose 1,6-bisphosphate breakdown, amino acid synthesis, and secondary metabolites; and SG decreasing genes related to starch and sugar metabolism, but increasing genes involved in oligosaccharide production and sugar modifications. Genes associated with flowering regulation within the photoperiod, vernalization, and meristem identity pathways were altered in these genotypes. Elevated $[CO_2]$ may act through carbohydrate changes to influence transcription in both genotypes and delayed flowering in SG. Changes in the oligosaccharide pool may contribute to delayed flowering in SG. This work extends the literature exploring genotypic-specific flowering responses to elevated $[CO_2]$.

Key words

Arabidopsis, elevated carbon dioxide, flowering time, Selected Genotype, carbohydrates, oligosaccharides

Introduction

Our planet is experiencing an increase in the concentration of atmospheric carbon dioxide ([CO_2]) that is unprecedented on the scale of evolutionary time. Atmospheric [CO_2] has increased from 270 ppm at the onset of the industrial age to a current value of 410 ppm due to fossil fuel combustion, and it is projected to increase to 700 ppm in the next 100 years [1]. This has implications for agricultural and ecological systems as plants have experienced relatively low [CO_2] over the last several million years, with minimums of 180 ppm occurring during peak glacial periods as recently as 20,000 years ago. One critical effect is changes in the timing of plant phenological events, including timing of peak flowering, which depending on the direction of change, may alter pollinator interactions [2–6], but see [7], or increase exposure to stressful climactic events such as spring frosts or summer droughts [2,8–11].

Much focus has been on warming temperatures occurring concomitantly with [CO_2] change (1.09 °C rise since 1850 [1]); however, recent evidence suggests that [CO_2] change contributes both independently and interactively with temperature to influence flowering time. For example, work with several field-collected *Arabidopsis thaliana* accessions isolated the separate and interactive effects of temperature and [CO_2] rise since the onset of the industrial era [12]. This work demonstrated that temperature and [CO_2] changes interacted to accelerate flowering in modern conditions compared to pre-industrial conditions. [CO_2] also independently influences flowering as a comprehensive review demonstrated that 57% of the wild species and 62% of the crop species tested exhibited changes in flowering times when grown at elevated [CO_2] (projected for year 2100) versus 350-380 ppm [CO_2] (modern levels) [13].

Currently, the patterns of [CO_2]-induced flowering time shifts are far from predictable as the magnitude and direction of changes in response to [CO_2] vary both intra- and interspecifically, and are modulated not only by temperature, but other environmental variables. Tested species showed accelerations, no change, or delays in flowering times in response to [CO_2] changes alone [13], and parallel ranges of response are observed within species. For example, in our work, two *Arabidopsis* strains from the same parental cross differed strikingly in their [CO_2]-induced flowering time responses. Although grown in the long-day conditions needed to induce flowering, a strain selected for high fitness, as measured by seed set, over successive generations in high [CO_2] (selected genotype, SG) delayed flowering by 10 d or more at elevated [CO_2] (700ppm) relative to 380 ppm. The control genotype (CG), that arose from random selection of individuals over successive generations, did not alter its flowering phenotype [14,15]. Similarly, near-isogenic soybean lines from the same genetic background differed in [CO_2] sensitivity, and the direction of change was modulated both by genotype and daylength [16]. Lines with dominance in single photoperiod genes accelerated flowering at elevated [CO_2] (560 ppm) in longer daylengths but delayed in shorter daylengths compared to modern [CO_2], while lines recessive across all photoperiod genes delayed flowering at elevated [CO_2] under all daylengths.

The mechanisms behind [CO_2]-induced flowering time changes and the variation in this response are unknown; however, alterations in the carbohydrate compositions in plant tissue likely contribute to this shift. Carbon dioxide concentration changes lead to marked changes in the rate of carbon accumulation through photosynthesis and in insoluble and soluble carbohydrates, downstream metabolites, and the carbon-to-nitrogen ratio across species

[17]. Further, alterations in both photosynthesis and carbohydrates composition have been linked to flowering. For example, *Lolium tremulentum* delayed flowering when treated with DCMU (3-(3,4-dichlorophenyl)-1,1-dimethylurea), a photosynthesis inhibitor [18], and floral induction coincides with a flux of carbohydrates from the leaves to the shoot apex [19–23]. Additionally, sucrose application in the growth media delayed flowering in *Arabidopsis*, a facultative long-day plant, with delay positively correlated to sucrose concentration [24]. The delay was caused by a longer vegetative phase, resulting in more leaves before flowering and was coupled with lower expression of the floral inducer genes *FLOWERING LOCUS T* (*FT*) and *LEAFY* (*LFY*). This behavior was similar to the delays in the soybean isolines at elevated [CO_2], which were associated with a higher number of nodes on the main stem, although carbohydrate content was not tested in that work [16].

Work in a wide range of organisms has highlighted a connection between carbohydrate or nutritional variation, downstream metabolic shifts, and global or targeted gene transcriptional regulation, providing possible specific mechanisms through which [CO_2] may influence developmental change. For example, in *Arabidopsis,* trehelose-6-phosphate (T6P) is responsive to sucrose levels and influences the expression levels of *FT* [25]. The authors proposed that T6P plays a role in signaling when carbohydrate reserves are sufficient to support the energy demands of reproduction. Additionally, a reversable post-translational sugar modification, O-linked B-N-acetylglucosaminylation (O-GlcNAcylation), is involved in the regulation of several transcriptional and epigenetic regulators including RNA polymerase II (Pol II) and Polycomb group (PcG) proteins across a variety of organisms [26–28]. It is linked to nutrition and carbohydrate-related diseases in humans such as *in utero* epigenetic responses in mothers exposed to famine or having Type-2 diabetes [26,29]. In plants, O-GlcNAcylation modulates the function of DELLA family proteins as well as expression of key flowering repressor gene *FLOWERING REPRESSOR C* (*FLC*) [30,31]. Both DELLAs and PcG proteins are involved in numerous endogenous and exogenous signaling pathways controlling plant environmental perception, development, and flowering time (e.g. [32–34]). Finally, the serine and glycine pools, downstream products of the Calvin cycle and glycolysis, shunt carbon through one-carbon metabolism to affect epigenetic regulation and such processes as cancer oncogenesis, further linking metabolism and nutrition to cell regulation [35,36]. In plants, the same process also acts downstream of the photorespiratory pathway to affect a range of processes including methylation and auxin synthesis and appears important for plant development and environmental response [37]. All three processes offer intriguing mechanisms that could not only influence [CO_2]-induced flowering time changes but explain how [CO_2]-driven responses are modulated by interactions with other environmental variables. Additionally, both standing levels of carbohydrates [38,39] and photosynthesis [40,41] and the degree to which they respond to different [CO_2] differ between and within species [41–44] even after just eight days of growth in elevated [CO_2] [45], thus suggesting a possible mechanism of intraspecific variation in response to [CO_2].

Compared to environmental processes such as daylength and temperature-mediated flowering time control [34,46–48], our knowledge of the molecular processes governing [CO_2]-driven flowering time shifts and the variation in that response is very much in its infancy (e.g. [15]). To begin to understand the mechanisms of [CO_2]-induced flowering time changes and the variation in this response, we utilize the CG SG system of *Arabidopsis* described above [15]. The CG SG system we describe above is a useful model, because as observed with *Arabidopsis* exposed to increasing concentrations of sucrose and soybean isolines exposed to elevated [CO_2]

[16,24], the delay in flowering in SG appears not only to be influenced by changes in the *rate* of growth and development, as would be expected from increased carbon acquisition through photosynthesis, but by alteration of the *developmental stage* (plant size and/or leaf number) at which plants flower. In our work, although SG developed more rapidly at elevated [CO_2] compared to current [CO_2], it flowered later because it produced more leaves before transitioning to the reproductive stage [15]. Conversely, CG flowered at a similar leaf number in both [CO_2]. This delay was correlated with prolonged high expression of the cold-responsive, flowering repressor gene *FLOWERING LOCUS C* (*FLC*) that acts upstream of *FT* only in SG grown in elevated [CO_2] [15]. In fall-germinating, winter-annual variants of *Arabidopsis*, *FLC* stays high until it is repressed by prolonged cold (=vernalization) [49] likely so that *FT* rises and flowering occurs appropriately in warm, spring conditions. In subsequent work, we confirmed that downregulation of *FLC* through vernalization restored early flowering in SG in elevated [CO_2] [50]. However, the upstream mechanisms governing the response of *FLC* to [CO_2] are unknown. Additionally, another flowering pathway may also be altered by [CO_2] change, as *LFY* was altered in both SG and CG, at least partially independently of *FLC* [15,50].

Here, by assessing the correlations between transcriptional and carbohydrate profiles and their relationship to known flowering time regulators, we aimed to evaluate through what metabolic pathways [CO_2] changes may be acting to influence flowering genes and flowering and how these processes differ between the genotypes at different [CO_2]. Thus, we harvested SG in current [CO_2], just prior to the visible transition to reproduction and SG in elevated [CO_2] at the analogous leaf number, but well before the reproductive transition. For comparison, we harvested CG in current and elevated [CO_2] just prior the reproductive transition as well. We specifically ask, how are carbohydrate profiles altered by [CO_2] across genotypes before flowering or at the analogous developmental stage in SG at elevated [CO_2], what transcriptional pathways correlate with the carbohydrate changes, and how does the [CO_2] response in SG vary from that of CG.

Results

Increased glucose and fructose correlates with elevated-[CO_2]-induced flowering delay in Selected Genotype

To assess carbon acquisition capacity of both the CG and SG lines at different [CO_2] and to determine the mechanisms responsible for genotype-specific flowering behaviors and the delay in flowering in SG, we compared primary carbohydrates—glucose, fructose, and sucrose—in CG just prior to production of a visible flowering stem (bolt) in current (380 ppm) and elevated (700 ppm) [CO_2], SG just prior to flowering at current [CO_2], and SG grown in elevated [CO_2] at the analogous developmental stage (leaf number), which was several days before it would transition to flowering (**Fig. 1**). To do so, we combined data from two experimental replicates that were detected through different methods (GCMS and NMR). To better compare across the two datasets and to be consistent with treatment of other data in this study, we transformed the data using centered-log ratio, then used ANOVA to assess effect of genotype, [CO_2] level, their interaction, and included replicate as a covariate. All three carbohydrates showed a clear effect of replicate; however, after variation for replicate was accounted for, glucose showed a significant [CO_2] effect ($p < 0.001$), fructose showed both a significant genotype and [CO_2] effect ($p < 0.01$, 0.001, respectively), and sucrose showed an effect of genotype ($p < 0.0001$). The genotype by [CO_2] interaction was not significant across the three carbohydrates. To assess the treatment groups driving these

differences, *post hoc* analysis revealed that SG had overall higher sucrose levels, with SG plants grown in 380 and 700 ppm being significantly higher than CG grown in 700 ppm ($p < 0.01$, 0.005, respectively), SG also had higher glucose levels driven by SG in 700 ppm being significantly higher than CG grown in 380 ppm ($p < 0.05$) (**Table 1**). Fructose showed the reverse, with SG in 380 ppm being lower than both CG in 380 and 700 ppm ($p < 0.05$, 0.0001, respectively). However, the effect of [CO_2] on glucose and fructose appears driven by SG. In both cases, SG grown in 700 ppm had higher levels than SG grown in 380 ppm ($p < 0.01$, 0.05, respectively), while the difference between [CO_2] treatments in CG was not significant (**Table 1**). In sum, SG appears to accumulate more glucose and sucrose relative to CG, especially in elevated [CO_2] when flowering in SG is delayed, and SG accumulates more glucose and fructose at 700 ppm [CO_2] than at 380 ppm, again correlating to a delay in flowering. The increase in primary carbohydrates in SG is consistent with previous observations in *Arabidopsis* as reviewed in [17]; as are the differences among genotypes in their standing levels and responses to [CO_2] [38,39,45]. Thus, carbon accumulation in the form of glucose and fructose may contribute to the delay in flowering in SG at elevated [CO_2]. More work is needed to determine whether higher sucrose concentrations are indicative of broader genotype sensitivity to [CO_2] in terms of phenological shifts.

Figure 1. Experimental set up. The Control and Selected Genotypes (CG and SG) were grown both at 'current' atmospheric [CO_2] **(**380 ppm) and projected future [CO_2] (700 ppm). Plants were harvested just prior to visible emergence of the reproductive stem (=bolt) for CG at 380 and 700 ppm, and for SG at 380 ppm. For SG at 700 ppm, plants were harvested at the analogous leaf number to SG grown at 380 ppm. Red and grey bars represent time. Leaf numbers shown are approximate. Bolt heights are exaggerated for visibility.

196 **Table 1:** Results of Tukey's Honest Significant Difference comparison for primary carbohydrates fructose, glucose,
197 and sucrose. *P* value adjusted for multiple comparisons and upper and lower 95% confidence interval bounds are
198 shown. **diff** = difference between the two treatments being compared in each row.

	Comparison	**diff**	**lwr**	**upr**	***p* adj**
Glucose	SG:380-CG:380	-0.0424	-0.3292	0.2445	0.9798
	CG:700-CG:380	0.1804	-0.0986	0.4594	0.3297
	SG:700-CG:380	0.3272	0.0403	0.6140	***0.0191***
	CG:700-SG:380	0.2228	-0.0604	0.5059	0.1725
	SG:700-SG:380	0.3695	0.0786	0.6604	***0.0072***
	SG:700-CG:700	0.1468	-0.1364	0.4299	0.5249
Fructose	SG:380-CG:380	-0.4555	-0.8331	-0.0779	***0.0118***
	CG:700-CG:380	0.2286	-0.1386	0.5959	0.3632
	SG:700-CG:380	0.0050	-0.3727	0.3826	1.0000
	CG:700-SG:380	0.6842	0.3114	1.0569	***0.0000***
	SG:700-SG:380	0.4605	0.0775	0.8434	***0.0121***
	SG:700-CG:700	-0.2237	-0.5964	0.1491	0.3960
Sucrose	SG:380-CG:380	0.5621	-0.1407	1.2650	0.1612
	CG:700-CG:380	-0.3468	-1.0304	0.3368	0.5429
	SG:700-CG:380	0.6542	-0.0486	1.3571	0.0771
	CG:700-SG:380	-0.9089	-1.6028	-0.2151	***0.0053***
	SG:700-SG:380	0.0921	-0.6208	0.8049	0.9863
	SG:700-CG:700	1.0010	0.3072	1.6949	***0.0018***

199
200 ***Bold, italicized text*** *in* p *adj.* column shows significant comparisons.
201
202
203
204

Selected and control genotypes vary in their transcriptional responses to [CO_2]

To further determine the mechanisms responsible for different flowering behaviors between CG and SG, we assessed whether transcriptional patterns, as detected through RNAseq and aligned to the Araport 11 reference genome, were altered between the genotypes and within the genotypes between [CO_2], using the same comparisons as with the primary carbohydrates, above. Originally, we detected 31,556 unique transcript identifiers across CG and SG. After removing poor-quality or low-count transcript identifiers, 16,472 transcript identifiers remained. We transformed the data using the centered-log ratio (clr) including all transcript counts within each sample in the denominator, as is recommended for compositional data [51,52], then calculated the Aitchison distances across all samples [53]. Note that as each transcript is centered relative to the geometric mean of all transcripts in that sample, values reported are relative to this within-sample control. At this stage, we compared samples based on their distances and found that one sample each from CG and SG grouped apart from the other samples in their strains (**Fig. S1**). These samples were removed as outliers and the distances recalculated. We, then, compared the relationships among the remaining sample distances using Principal Components Analysis (PCA) and permuted multivariate ANOVA (PERMANOVA), with the latter assessing the effects of genotype, [CO_2], and their interaction. Principal Component 1 (PC1) explained 65.6% of the variation, and this was largely driven by genotype (**Fig. S2a**). No clear pattern based on genotype or [CO_2] treatment emerged across PC2, which explained 11.1% of the variation; however, SG showed a clear separation between [CO_2] treatments relative to CG across PC3, which explained 5.3% of the variation (**Fig S2b**). Consistent with this pattern, PERMANOVA revealed a significant genotype effect and genotype-by-[CO_2] interaction ($p < 0.001$, 0.05, respectively).

To assess the transcripts driving these patterns, we conducted differential expression analysis of each identified transcript. For these, we assessed whether there was an effect of genotype and [CO_2], and report those with an effect size greater than ± 1 [52]. Between genotypes, 3616 fit this condition (**Fig. 2a-b, Table S1**). For, [CO_2] only 48 genes showed an effect size greater than ± 1, with 39 of those showing a decrease relative to the internal control in elevated [CO_2] (**Table S1**). We used functional annotation clustering to determine the probable function of these altered transcripts (**Table 2 & S2a-d**). This process pulls annotation terms from multiple resources and clusters those terms based on whether they overlap in the genes used to call those terms. For those genes showing strong effect sizes across genotypes and being higher in SG than CG relative to the internal control, the top five functional clusters were: serine/threonine and protein kinase activity; transmembrane or membrane components; calcium-binding region, serine/threonine kinase, peptidyl-serine phosphorylation; signal transduction; ADP and DNA binding, leucine-rich repeats; and ankyrin repeat and PGG domains. For those genes lower in SG than CG, the top five functional clusters were: chloroplast related; ribosome related; chloroplast thylakoid lumen related; ribosomal RNA-binding related; and lipid biosynthesis and metabolism related. For the effect of [CO_2], when analyzed across genotype, no significant functional annotations emerged (**Table S2d**).

239 **Table 2:** Summary table of top five functional annotation clusters in each comparison.

Comparison	Functional Annotation Clusters	Enrich. Score	Unique gene IDs
Genotype	Serine/threonine and protein kinase activity	21.43	1573
Increase from CG to SG	Transmembrane or membrane components	11.93	
	Calcium-binding region, serine/threonine kinase, peptidyl-serine phosphorylationsignal transduction	7.5	
	ADP and DNA binding, leucine-rich repeats	5.68	
	Ankyrin repeat and PGG domains	5.55	
Genotype	Chloroplast	172.46	1987
Decrease from CG to SG	Ribosome	37.42	
	Chloroplast thylakoid lumen	19.91	
	Ribosomal RNA-binding	9.38	
	Lipid biosynthesis and metabolism	6.11	
CG *Increase from 380 to 700 ppm*	Transit peptide, chloroplast thylakoid membrane	20.13	701
	PSI, PSII, chlrophyll a/b, chloroplast, magnesium binding	12.17	
	Membrane, transmembrane	5.89	
	Glycolysis/gluconeogenesis, biosynthesis of amino acids/antibiotics	4.38	
	Cytochrome b5 heme-binding	3.87	
CG	ATP and nucleotide binding	4.93	292
Decrease from 380 to 700 ppm	Microtubule motor protein activity	4.39	
	Nucleus, sequence-specific DNA binding, and transcription regulation	4.35	
	Cell division and mitosis	3.55	
	Zinc and metal binding	2.76	
SG *Increase from 380 to 700 ppm*	Golgi related and glycosyl and hexosyl transferase activity	3.75	226
	Small GTP binding and GTPase-mediated signal transduction	2.83	
	Cytoskeleton and microtubule	2.71	
	Cell wall organization	2.24	
	IQ motif and calmodulin binding	1.79	
SG	Chloroplast and transit peptide	82.03	1017
Decrease from 380 to 700 ppm	Carbon metabolism and fixation, biosynthesis and metabolic pathways	5.42	
	Thylakoid, ATP- and metallo-peptidase activity, photoinhibition and PSII repair and catabolic processes	4.92	
	ATP-dependent peptidase activity and PUA-like domain	4.55	
	Transmembrane components	4.21	

To better understand the transcripts driving the significant interaction observed in the PERMANOVA as genotype was such a strong determinant of differences in transcript profiles, we next assessed the effect of [CO_2] for each genotype individually (**Fig. 2c-f, Table, S1 & S2a,e-h**). CG showed 995 transcripts with a large effect size with most increasing from 380 to 700 ppm [CO_2], while SG showed 1273 transcripts with a large effect size with most decreasing from 380 to 700 ppm [CO_2]. For those increasing in CG (**Fig. 2c, Table 2, S1 & S2a,e**)., the top five functional annotation clusters were: transit peptide, chloroplast thylakoid membrane; PSI, PSII, chlorophyll a/b, chloroplast, magnesium binding; membrane, transmembrane; glycolysis/gluconeogenesis, biosynthesis of amino acids/antibiotics; cytochrome b5 heme-binding. Each of these clusters also included the annotation terms 'plastid', 'chloroplast thylakoid', 'chloroplast envelope', 'Chlorophyll-a 5', and 'Chlorophyll-a 5', respectively, potentially indicating that much of the increased transcript activity within CG at elevated [CO_2] was associated with photosynthetic structures. For those decreasing in CG (**Fig. 2d, Table 2, S1 & S2a,f**)., the top five clusters were: ATP and nucleotide binding; microtubule motor protein activity; nucleus, sequence-specific DNA binding, and transcription regulation; cell division and mitosis; and zinc and metal binding. For those transcripts increasing in SG (**Fig. 2e, Table 2, S1 & S2a,g**)., the top five clusters were: Golgi related and glycosyl and hexosyl transferase activity; small GTP binding and GTPase-mediated signal transduction; cytoskeleton and microtubule associated; cell wall organization; and IQ motif and calmodulin binding. For those decreasing in SG (**Fig. 2f, Table 2, S1 & S42a,h**)., the top five clusters were: Chloroplast and transit peptide; carbon metabolism and fixation, biosynthesis and metabolic pathways; thylakoid, ATP- and metallo-peptidase activity, photoinhibition and PSII repair and catabolic processes; ATP-dependent peptidase activity and PUA-like domain; and transmembrane components.

Figure 2. Transcript count differed between the Control and Selected Genotypes (CG and SG) and within genotypes across 380 and 700 ppm [CO_2]. **(a-f)** Each grey line (background) represents the mean relativized count (centered log ratio) of the 16,472 unique transcript identifiers in this dataset. Colored lines in **bold** represent those transcript identifiers with effect sizes greater than $\pm$ 1 in each comparison, while the lighter sections in each plot allow visualization of how those same transcripts respond across genotypes or within the other genotype. **(a-b)** Transcript identifiers showing an increase **(a)** and decrease **(b)** from CG to SG. **(c-d, bold lines)** Transcript identifiers showing an increase **(c)** and decrease **(d)** in CG from 380 to 700 ppm [CO_2]. For reference, the same transcripts are visible in SG (light lines). **(e-f, bold lines)** Transcript identifiers showing an increase **(e)** and decrease **(f)** in SG from 380 to 700 ppm [CO_2]. For reference, the same transcripts are visible in CG (light lines). Green lines in **d-f** show flowering genes found to have effect sizes greater than $\pm$ 1.

Many of the significant clusters for each comparison had overlapping annotation categories (**Table 2, S2a-h**), so to better characterize overarching functional descriptions we used both manual categorization and word-cloud generation (worditout.com) to assess patterns across all significant annotation clusters. These categorization processes revealed that there was an increase from CG to SG, relative to the internal control, in serine/threonine protein phosphorylation and signaling, glycoprotein and glycosylation signaling, and Golgi and vesicle transport. Thus, the two genotypes have different signaling cascades at the developmental stage just prior to flowering.

Conversely, there was a decrease from CG to SG in photosynthetic and energy transfer (redox) processes. This appeared most strongly driven by down-regulation of photosynthesis related genes in SG from 380 to 700 ppm as CG and SG displayed nearly opposite patterns of gene regulation from 380 to 700 ppm. For instance, CG increased genes involved in processes related to photosynthesis, energy transfer, and metabolite breakdown and biosynthesis. Thus, CG may capitalize on available carbon in a high [CO_2] environment by increasing carbon acquisition and processing. Conversely, SG decreased genes involved in processes related to PSII repair and photoinhibition, energy transfer (i.e. FAD/NADPH), and carbon fixation and metabolite biosynthesis. Perhaps, under current [CO_2], SG experiences some photoinhibition which is alleviated by increased CO_2 availability as has been shown for other species when nutrients are not limiting [54,55]. Further, while CG decreased genes involved in processes related to nucleotide binding, cell division, and cell reorganization and internal transport (i.e. motor proteins and nuclear pores), SG increased genes involved in processes related to cellular internal transport (i.e. motor proteins and Golgi vesicles), and sugar signaling and processing (i.e. glycosyl transferase, polysaccharide binding). Thus, when SG is not preparing to flower at elevated [CO_2], it is maintaining relatively higher intercellular signaling and motility. It is unknown from our current design whether such behavior would be observed in SG grown at 380 ppm well before flowering is initiated.

Control and Selected Genotypes display differing metabolic responses to elevated [CO_2]

As CG showed no clear [CO_2] response in primary carbohydrate levels yet displayed strong changes in carbohydrate-related genes, we wondered whether other metabolites were being altered in CG. We assessed 15 additional metabolites common across the NMR and GCMS data sets (**Table S3**), assessing the effect of [CO_2] independently within each genotype as the effect of genotype was very strong, and incorporating dataset as a covariate. We noted differing carbohydrate profiles for each genotype, with CG showing significant increases in glucose-6-phosphate, succinic acid, and trehalose, and decreases in aspartic acid, glycine, and threonine. In addition to increases in glucose and fructose, SG showed increases in succinic acid and trehalose, and decreases in glutamine and serine (**Table S3**). Thus, while CG does not show a strong response to [CO_2] in primary carbohydrates glucose and fructose, CG does display an altered carbohydrate profile in response to [CO_2] change, although this does not correlate with altered flowering in this genotype.

Genes involved in sugar modifications and one-carbon metabolism altered in Selected Genotype

To better assess potential pathways contributing to delayed flowering in SG in response to elevated [CO_2], we explored genes within the carbohydrate-related functional annotation clusters in more detail. We did this through a manual referencing of genes in significant clusters to The Arabidopsis Information Resource (TAIR, [56]), and by searching the clusters for genes involved in the trehalose-6-phosphate, O-GlcNAcylation, and one-carbon metabolism pathways (**Table 3**). SG showed an increase in several genes encoding O-glycosyl hydrolases including AT5G55180, AT3G55430, and AT5G08000 (also called *E13L3*) (**Table 3**). Per TAIR [56], these genes enable cleavage at internal 1,3-beta-D-glucose linkages (endo-1,3-beta glucosidases) to cause the formation of oligosaccharides. It is possible that the cleaved oligosaccharides participate in a signal cascade serving as secondary modifications to protein- or lipid-based molecules. For instance, several sugar transferases were also positively

316 enriched in SG plants grown at 700 ppm [CO_2]. These included AT3G21190 (ATMSR1), an O-fucosyltransferase;
317 AT2G28080, a UDP-glycosyltransferase; and AT3G58790 (GAUT15), a galacturonosyltransferase, among others
318 (**Table 3**). We also noted that genes associated with one-carbon metabolism, which involves the addition or removal
319 of single carbon units and which is involved in a range of metabolic, epigenetic, or transcriptional regulatory
320 processes [37,57], displayed differences across groups. We focused on genes involved in the process of methylation,
321 which is involved in transcriptional and epigenetic regulatory processes [36,58]. Several methyltransferases were
322 included in this data set and two of these—AT4G37930 and AT5G13050—declined in SG in response to elevated
323 [CO_2] (**Table 3**). Several genes act upstream in this pathway to generate S-adenosyl-Met ([59] in [57]) which serves
324 as a methyl group donor for methyltransferase reactions. These are cystathionine gamma-synthase (*CGS*),
325 cystathionine beta-lyase (*CBS*), and methionine synthase; all of which are located in the chloroplast [57] explaining
326 their presence in clusters associated with that term (**Table S2h**). *CGS* (AT3G01120) was lower in SG relative to CG,
327 as was a threonine synthase (*MTO1*, AT3G01120). Additionally, *MTO2* showed a within genotype effect to [CO_2] as
328 it decreased in SG in elevated [CO_2] relative to current [CO_2] conditions (**Table 3, S1**). Threonine synthase
329 competes with *CGS* for the substrate *O*-phosphohomo-Ser (OPH) [57]. As *MTO2* decreases in response to elevated
330 [CO_2] in SG, it is possible that OPH is being used to generate S-adenosyl-met for methyltransferase reactions,
331 despite both *CGS* and *MTO1* being relatively lower in SG than in CG (**Table S1**). Thus, increased production of
332 both oligosaccharides and single-carbon molecules may occur in SG, correlating with a delay in flowering in
333 elevated [CO_2]. However, as two methyltransferases decreased in SG while several sugar transferases increase,
334 signaling pathways involving oligosaccharides may contribute to the flowering delay.
335

336 **Table 3:** Details of genes found within functional annotations associated with carbohydrate-related processes.

	TAIR ID	Entrez ID	Gene Name
Increase	AT3G21190	821672	O-fucosyltransferase family protein (*MSR1*)
	AT3G03050	821148	Cellulose synthase-like D3 (*CSLD3*)
	AT2G28080	817352	UDP-Glycosyltransferase superfamily protein
	AT3G58790	825048	Calacturonosyltransferase 15 (*GAUT15*)
	AT1G24170	839030	Nucleotide-diphospho-sugar transferases superfamily protein (*LGT9*)
	AT1G32930	840187	Galactosyltransferase family protein
	AT5G65470	836672	O-fucosyltransferase family protein
	AT1G11730	837717	Galactosyltransferase family protein
	AT5G12970	831137	Calcium-dependent lipid-binding (CaLB domain) plant phosphoribosyltransferase family protein
	AT1G23480	838956	Cellulose synthase-like A3 (*CSLA03*)
	AT5G57500	835854	Galactosyltransferase family protein
	AT1G74380	843779	Xyloglucan xylosyltransferase 5 (*XXT5*)
	AT5G16190	831477	Cellulose synthase like A11 (*CSLA11)*
Decrease	AT2G26080	817149	Glycine decarboxylase P-protein 2 (*GLDP2*)
	AT3G02880	821198	Leucine-rich repeat protein kinase family protein
	AT3G55430	824709	O-Glycosyl hydrolases family 17 protein
	AT2G47390	819352	Prolyl oligopeptidase family protein
	AT5G46390	834682	Peptidase S41 family protein
	AT4G36190	829776	Serine carboxypeptidase S28 family protein
	AT5G48450	834900	SKU5 similar 3 (*SKS3*)
	AT4G29840	829106	Pyridoxal-5'-phosphate-dependent enzyme family protein (*MTO2*)
	AT5G47040	834750	Lon protease 2 (*LON2*)
	AT5G08000	830694	Glucan endo-1,3-beta-glucosidase-like protein 3 (*E13L3*)
	AT4G12880	826900	Early nodulin-like protein 19 (*ENODL19*)
	AT3G27925	822416	DegP protease 1 (*DEG1*)
	AT5G39830	833979	Trypsin family protein with PDZ domain-containing protein (*DEG8*)
	AT2G02850	814816	Plantacyanin (*ARPN*)
	AT5G13050	831144	5-formyltetrahydrofolate cycloligase (*5-FCL*)
	AT4G37930	829949	Serine transhydroxymethyltransferase 1 (*SHM1*)
	AT4G33010	829438	Glycine decarboxylase P-protein 1 (*GLDP1*)
	AT5G55180	835611	O-Glycosyl hydrolases family 17 protein
	AT3G15720	820815	Pectin lyase-like superfamily protein
	AT4G34120	829558	Cystathionine beta-synthase (CBS) family protein (*LEJ1*)

337
338

We also determined whether genes from two other carbohydrate-related pathways and associated with flowering differed in this dataset. For genes influencing trehalose-6-phosphate (T6P) [25], eight of the eleven *T6P SYNTHASE* (*TPS*) genes and six of the ten *T6P PHOSPHATASE* genes (reviewed in [60]) were present in this dataset. However, while two T6P-related genes differed between genotypes, only one showed a within-strain [CO_2] response (**Table S1**). Specifically, AT1G23870 (*TPS9*) decreased from ambient to elevated [CO_2] in CG; while two members of the ten-member *T6P PHOSPHATASE* family—AT5G65140 (*TPPJ*) and AT2G22190 (*TPPE*)—decreased and increased in SG relative to CG, respectively. Thus, differences in *T6P*-related genes were not observed in SG; although it is important to note that *TPS2, TPS3, TPS4*, *TPPC*, *TPPE*, *TPPG*, and *TPPI* were not included in the dataset. *TREHELASE* (*TRE1*) [61], also included in the dataset, did not show an effect. The T6P pathways interacts with the pathway involving *SUCROSE NON-FERMENTING1-RELATED KINASES* (*SnRK1*, also *KIN10*, AT3G01090) [62], which also influences flowering [63]. While both *KIN10* and related *KIN11* (AT3G29160) [64] were higher in SG than in CG, neither was affected by [CO_2] change within a genotype (**Table S1**). Secondly, we assessed the genes involved in serine/threonine-linked glycosylation, O-GlcNAcylation [31]. *SECRET AGENT* (*SEC*, AT3G04240) the primary O-GlcNAc transferase in *Arabidopsis*, did not show a large effect size in any of the comparisons made in this work. *SPINDLY* (*SPY*, AT3G11540), an O-fucosyltransferase originally predicted as an O-GlcNAc transferase and which acts within the same regulatory pathways [30,65–67], also did not differ. Thus, these pathways appear not to correspond to the flowering delay in SG.

Carbohydrate-responsive flowering regulator genes differ in response to [CO_2] change

The observed differences between genotypes and between the [CO_2] treatments, primarily in photosynthetic and carbohydrate related processes, are consistent both with the differences in primary carbohydrates we observed, and with the range of photosynthetic and carbohydrate responses observed elsewhere [17]. However, as we were interested in mechanisms controlling flowering, and whether there was a relationship between carbohydrate-mediated pathways and flowering-control mechanisms, we also assessed whether there were differences in the flowering genes independently. We assessed a list of 156 genes known to be associated with flowering [68] (**Table S4**), of which 125 matched transcripts in this dataset (**Table S4**). These included components of the circadian clock, photoperiod, ambient temperature, vernalization, endogenous, and meristem identity flowering control pathways. In CG, there were six genes with effect sizes greater than $\pm$ 1, all showing a relative decrease from current to elevated [CO_2]. These were *ARABIDOPSIS TRITHORAX 2* (*ATX2*); *FRIGIDA* (*FRI*); *AGAMOUS-LIKE 24* (*AGL24*); *GATA, NITRATE-INDUCIBLE, CARBON METABOLISM INVOLVED* (*GNC*); *FRUITFULL* (*FUL*); and *TIMING OF CAB EXPRESSION 1* (*TOC1*). Both *ATX2* and *FRI* regulate the vernalization-responsive, flowering repressor *FLOWERING LOCUS C* (*FLC*), which was previously shown to be strongly elevated in SG under elevated [CO_2] [15,50], and slightly elevated in CG early in development before declining prior to flowering in a subsequent experiment [50]. *ATX2* is a set-domain-containing protein required for H3K4 methylation and activation of *FLC* [69], while *FRI* complexes with transcriptional and chromatin-modifying factors to induce *FLC* [70]. The MADS-box encoding *AGL24* and *FUL* are floral meristem identity genes downstream of *FLC* and another MADS-box encoding floral regulator gene *SUPPRESSOR OF OVEREXPRESSION OF CONSTANS 1* (*SOC1*) [68], which was previously shown to be suppressed in SG in response to elevated [CO_2] [15,50] and which was upregulated in SG in

elevated [CO_2] in response to prolonged cold temperatures (vernalization) [50]. *SOC1* is also downstream of *FLC*, which is well known to regulate response to winter temperatures and is repressed by vernalization [71]. Vernalization restored earlier flowering in SG in elevated [CO_2] [50]. *AGL24* interacts with *SOC1* to regulate another meristem identity gene, *LEAFY* (*LFY*) [72], which was previously shown to be upregulated by elevated [CO_2] in both genotypes either independently or interactively with prolonged cold treatment (vernalization) [15,50]. *LFY* and *FUL* are regulated by micro RNA 156-regulated SPL transcription factors [73,74], which in turn, are modified by T6P [25], suggesting one mechanism through which [CO_2]-induced carbohydrate changes may alter flowering. Additionally, *GNC*, known to be involved in stomatal and chloroplast development, glucose sensitivity, and leaf starch level [75–78], regulates *SOC1* and flowering [79,80]. Finally, *TOC1*, is a component of the *Arabidopsis* circadian clock [81], which acts through the photoperiod sensing pathway to regulate flowering time [82,83]. The circadian clock regulates plant metabolic state by regulation of photosynthesis and starch breakdown [84,85] but is carbohydrate responsive as well [86,87]. Thus, although CG does not visibly alter its flowering time in response to [CO_2], several flowering-regulator genes are altered, many of which have known links to carbohydrate response pathways and to previous responses to [CO_2].

In SG, there were four genes with effect sizes greater than $\pm$ 1, with three showing a relative decrease from current to elevated [CO_2] and one showing an increase. Those showing a decrease were *SUPPRESSOR OF PHYA-105 3* (*SPA3*), *BOTRYTIS SUSCEPTIBLE 1 INTERACTOR* (*BIO*), and *CONSTANS* (*CO*). The one showing an increase was *TEMPRANILLO 2* (*TEM2*). *CO* is a key, circadian-regulated component of the photoperiodic-sensing pathway and upstream inducer of the floral integrator gene, *FLOWERING LOCUS T* (*FT*) [88–90]. The SPA1, SPA3, and SPA4 proteins redundantly degrade CO protein in the dark, ensuring delayed flowering in short-photoperiod conditions [91–94]. *BIO* represses flowering by repressing *FT* through both *CO*-dependent and -independent mechanisms [95]. *TEM2*, along with *TEM1*, acts to repress *FT* antagonistically to CO, with TEM1 recruiting Polycomb factors to the *FT* locus [96,97]. Both *BIO* and the *TEM* genes are associated with the gibberellin pathway [98,99], and several members of the gibberellin-response pathway appear also to be involved in plant carbohydrate regulation and flowering time [100]. Thus, across both genotypes, genes within the photoperiod, vernalization, and meristem identity response pathways are altered in response to [CO_2].

Discussion

Here, we aimed to assess potential metabolic pathways through which [CO_2] change may alter flowering genes and flowering times and to determine mechanisms for genotypic variation in flowering response. We found that prior to flowering, the *Arabidopsis* Selected Genotype (SG) that delays flowering when exposed to elevated [CO_2] had higher sucrose levels relative to the Control Genotype (CG) that does not show a [CO_2]-induced flowering phenotype. SG also responds more strongly than CG to a [CO_2] increase by increasing glucose and fructose levels. This pattern is consistent with the delay in flowering in *Arabidopsis* observed over increasing sucrose concentrations in plant growth media [24]. Thus, higher sugar content in the form of glucose and fructose may contribute to the flowering delay in SG in response to elevated [CO_2]. *Arabidopsis* accessions display substantial variation in carbon accumulation and photosynthetic capacity in general [101] and the degree to which these traits respond to [CO_2] and temperature change [45,102]. As SG appears to respond more strongly to [CO_2] change by altering these foliar

carbohydrates, capacity to accumulate higher glucose and fructose could be an indicator of flowering time change in response to [CO_2] rise. Finally, it is also possible that higher sucrose accumulation as observed in SG indicates likelihood to delay flowering. However, while both CG and SG were collected at analogous developmental stages (i.e. before the reproductive transition), SG was collected at a higher leaf number. Thus, subsequent studies exploring change in carbohydrate accumulation over time will be useful, as will experiments assessing whether these patterns hold across a broad range of accessions.

A large body of work now demonstrates the connection between transcriptional and epigenetic regulatory processes and carbohydrate levels in both plants and animals (as reviewed in [36,103]). Small soluble sugars such as glucose and fructose serve direct signaling functions [103], but carbohydrates also serve as protein post-translational modifications and as substrates for protein and histone methylation [36,103]. In animals, these processes link the nutrition or disease state of an organism to the genome to elicit a response [26,104]. In plants, these processes likely link not only the endogenous environment but the external environment to the genome as carbohydrate levels in plant tissue are altered by cold temperatures [105,106], drought [107,108], salinity [109,110], daylength and light levels [20,111], and herbivory [112] to name only a few environmental variables. Thus, it stands to reason that changes in carbohydrate composition and level would be the mediating factor through which change in atmospheric [CO_2], the primary photosynthetic substrate, alters developmental responses such as the timing of the vegetative to reproductive transition. Here, during the developmental stage prior to flowering, both CG and SG displayed alterations in genes related to metabolic processes in response to elevated [CO_2] relative to current [CO_2]. However, the two genotypes differed in the processes altered. CG increased genes related to breakdown of fructose 1,6-bisphosphate (fructose-bisphosphate aldolase) and the synthesis of amino acids and secondary metabolites. Conversely, in response to a rise in [CO_2], SG showed a decrease in genes related to starch and sugar biosynthesis and metabolism, but increased genes involved in production of oligosaccharides and in sugar modifications (glycosyl and hexosyl transferase, polysaccharide binding). Additionally, one of the threonine synthases (*MTO2*) present in the data set decreased in response to elevated [CO_2] in SG. These enzymes competitively inhibit reactions involved in the production of S-adenosyl-Met, which donates methyl groups for methyltransferase reactions [57]. Thus, increases in oligosaccharide pools and potentially the pool of S-adenosyl-Met correlate with delayed flowering in SG in response to elevated [CO_2]. The oligosaccharide pool is likely contributing to a signaling cascade as glycosyl and hexosyl transferases also increase. However, as small sugars can act independently or modify both proteins and lipids [103], whether the oligosaccharide increase is influencing specific pathways or acting more generally is an open question.

Finally, as we were interested in the flowering regulatory mechanisms correlating with differences in [CO_2] response in these genotypes, we explored flowering-related genes specifically and noted that several genes representing the vernalization, photoperiod, and meristem identity pathways were altered in either CG or SG in response to [CO_2] change. Although CG shows no flowering time phenotype in response to elevated [CO_2], flowering genes *FLC*, *SOC1*, and *LFY* were shown to be altered in previous studies using these lines, and genes associated with all three were altered in CG here. We noted differences in *ATX2* which appears to act semi-redundantly with *ATX1* to regulate *FLC* expression [113], but may play more of a role later in development as *pATX2:GUS* was expressed in older leaves while *pATX1:GUS* was expressed throughout development [114].

Although, to our knowledge, *ATX2* has not yet been associated with carbohydrate changes, *ATX1* is regulated by O-GlcNAcylation [31] and *ATX5* is glucose responsive [115]. Thus, *ATX2* may respond to [CO_2]-induced foliar carbohydrate changes to influenced *FLC* at least in CG. We also noted alterations in *AGL24* and *GNC* which interact with *SOC1*, a gene upstream of *LFY* [72,80]. Here, we noted alterations in *FUL* as well. Per the Flowering Interactive Database, *LFY* and *FUL* are both regulated by *SOC1* [68], but are also regulated by *SPL* transcription factors which are influenced by T6P [25,73,74]. Although T6P-related genes were not altered in SG in response to [CO_2] change, *TPS9* was altered in CG. *TPS9* seems not to act enzymatically to affect *T6P* levels, but may serve a regulatory function in response to carbohydrates and is repressed by sucrose and glucose [116] consistent with its decrease from current to elevated [CO_2], here. While we did not observe altered sucrose, glucose, or fructose in response to [CO_2] change in CG, other carbohydrates did increase with elevated [CO_2] in that genotype including glucose-6-phosphate and trehalose, perhaps leading to the changes observed here. Finally, the circadian clock gene *TOC1* regulates the photoperiod-sensing pathway upstream of *SOC1*, *LFY*, and *FUL* [68]. The circadian clock is also regulated by carbohydrates [86,87], demonstrating that [CO_2] rise may influence the expression profiles of several flowering-related pathways.

Although the vernalization response pathway in addition to other floral integrator genes has been shown to be important for the [CO_2]-induced delay in SG [15,50], we did not note vernalization response genes to be altered here in SG. However, we noted that genes involved in the photoperiod and gibberellin-response pathways were altered. These genes all act upstream of the key floral integrator genes, *FT*, *LFY*, and *SOC1*, and also have connections to carbohydrates. For instance, the SPAs contain a serine/threonine protein kinase domain that, in SPA1, has recently been shown to be necessary for photomorphogenic response [117]. Protein phosphorylation and the protein sugar modification, O-GlcNAcylation, both target serine and threonine amino acids and are known to both compete for and influence the other [118]. Additionally, the SPAs redundantly complex with *CONSTITUTIVE PHOTOMORPHOGENIC 1* (*COP1*) to degrade CO protein in the dark [91–94]. PHYTOCHROME A disrupts the COP1/SPA complex to allow light-promoted flowering; however, COP1/SPA may feedback to degrade PHYA in a manner that is dependent on sugar [119,120]. Additionally, *CO*, *COP1*, and the *SPA* family are all regulated by the circadian clock, a process that is also influenced by carbohydrates [86,87]. Additionally, both *BIO* and *TEM* genes are involved in the gibberellic (GA) sensing pathway, which is associated with sugar sensing at several points. For instance, GA and sucrose were implicated early in their interactive activation of *LFY* [121], and the *TEM* genes directly regulate genes involved in GA biosynthesis as well as influence the expression of *FT* which acts upstream of *LFY* and other flowering-transition genes [68,99]. Further, BIO and DELLA proteins interact to regulate GA-responsive genes [98], while *GIGANTEA* (*GI*), a key circadian clock gene, stabilizes the DELLA proteins to gate GA-response to the night [122]. The DELLAs are post-translationally modified by O-GlcNAcylation, while *GIGANTEA* is involved in sugar-sensing and in sugar regulation of the circadian clock [123]. Whether *BIO* and *TEM2* transcription is influenced either directly or indirectly by sugars is, to our knowledge, not known. However, in rice, sugar starvation directly influenced a regulator of genes involved in GA biosynthesis [124]. Thus, across CG and SG, our study highlights several additional candidate flowering-control pathways responsible for flowering time variation in response to [CO_2].

It should be noted that while we had observed the key vernalization-responsive, floral-repressor gene, *FLC*, to prolong its elevated expression in SG and that its expression contributed to flowering delays [15,50], *FLC* did not show differences in either CG or SG at the time point harvested, here. This may be due to the detection method used as we noted significant variation among samples. Additionally, the flowering genes, overall, showed a much lower degree of response than genes related to carbohydrate pathways and therefore differences detected by exploring these genes individually may not be detected through a transcriptomics approach. Further, while several genes upstream of key floral integrators *FT* and *LFY* were altered in our dataset, neither *FT* nor *LFY* were included in the dataset. Finally, regulation of these genes is complex, with several cycling over a 24-hour period as regulated by the circadian clock [68] or changing throughout development as is the case of vernalization-responsive genes [34]. Thus, much more work needs to be done to understand the relative influence of the different flowering pathways shown to be altered here and the degree to which they interact. Further experiments assessing their degree of change over developmental and diurnal time will be necessary.

In sum, this study coupled with our two previous studies paints a picture in which atmospheric [CO_2] change influences carbohydrate response pathways, which in turn influence flowering regulators to alter flowering in a genotype-specific manner. This study highlights additional candidate pathways responsible for flowering variation in response to atmospheric [CO_2] change.

Materials and Methods

Plant Material and Growth Conditions

We used our novel *Arabidopsis* system involving two genotypes [14,15,125], whereby genotype SG delays flowering at elevated [CO_2] and flowers at a larger size, and genotype CG exhibits similar flowering times and size at flowering between 380 and 700 ppm [CO_2]. These genotypes were originally generated from the same parental cross. SG was generated through selection over consecutive generations of growth at elevated [CO_2], by choosing individuals with high seed set [14]. CG was generated through selection of random individuals at each generation. We assessed carbohydrate, metabolite, and transcriptomic responses in rosettes leading up to flowering in SG and CG plants grown at 380 and 700 ppm [CO_2] (**Fig. 1**). For SG, these measurements were taken prior to the initiation of reproduction at 380 ppm [CO_2] as well as the analogous stage (leaf number) during growth at 700 ppm when plants should flower (as in 380 ppm), but do not (see **Fig. 1** for harvesting regime). Sample size (n) was five to nine plants per genotype for both metabolomic and transcriptomic analyses. Flowering was defined as the visible transition from vegetative to floral growth of the meristem (i.e. the flowering stem was visible above the rosette). Signal plants were planted out one week prior to the plants used in the experiment, such that when the signal plants visibly transitioned to reproduction, the plants used for the experiment were harvested. Rosette leaf numbers were counted at harvest and cotyledons were excluded from these counts.

We utilized Conviron BDR16 (Winnepeg, Canada) growth chambers with custom control of [CO_2], in which [CO_2] was automatically injected when needed and chamber air was pulled through JorVet soda lime (Loveland, CO, U.S.A.) to scrub excess [CO_2]. Chambers constantly monitored internal conditions and [CO_2] was maintained at ±20 ppm of either 380 or 700 ppm at least 95% of the time. Temperatures were set at 25/18 °C

day/night and humidity was set at 60/90% day night. Seeds were cold stratified at 4 °C for four days prior to beginning the experiment to promote uniform germination. Plants were grown under 14-hour photoperiods with light levels ~800 µmol m-2 s-1 in 750 mL pots filled with a 1:1:1 (v/v) mixture of pea gravel, vermiculate, and Terface (Profile Products, Buffalo Grove, IL, U.S.A.). All plants were well watered and dosed with half-strength Hoagland's Solution (**Table S5**) daily.

Carbohydrate and Metabolite Profiling

In collaboration with the Ecological and Molecular Sciences Laboratory (EMSL) at the Department of Energy Pacific Northwest National Laboratory EMSL, we measured total leaf sucrose, glucose, fructose and related metabolites during time points leading up to flowering in SG and CG plants grown at 380 and 700 ppm [CO_2]. For NMR, *Arabidopsis thaliana* frozen leaf tissues were weighed and ground by using two 3 mm stainless steel beads for 3 minutes at 30 Hz with frozen adapters on a TissueLyser II (Qiagen). The resulting frozen powder was dissolved in 650 µL chloroform-methanol (3:7, v/v) and placed in the -20 °C freezer with occasional shaking for 2 hours. Next, 600 µL of ice-cold nanopure water was added and placed in the 4 °C fridge with repeated shaking for 15 minutes. Finally, the sample was centrifuged at 12,000 rpm for 5 mins, the aqueous phase was collected and dried in the speed-vacuum concentrator. The NMR sample of *Arabidopsis* was dissolved in 600 µL of H_2O-D_2O (9:1,v/v) with 0.5 mM DSS.

All NMR spectra were collected using a Varian Direct Drive 600 MHz NMR spectrometer equipped with a 5 mm triple-resonance salt-tolerant cold probe. The 1D 1H NMR spectra of all samples were processed, assigned, and analyzed by using Chenomx NMR Suite 8.1 with quantification based on spectral intensities relative to the internal standard. Candidate metabolites present in each complex mixture were determined by matching the chemical shift, J-coupling, and intensity information of experimental NMR signals against the NMR signals of standard metabolites in the Chenomx library. The 1D 1H spectra were collected following standard Chenomx data collection guidelines [126], employing a 1D NOESY presaturation experiment with 65536 complex points and at least 512 scans at 298 K. Additionally, 2D ^{13}C-^{1}H HSQC spectra were collected with N1=1024 and N2=1024 complex points. The spectral widths along the indirect and direct dimension were 160 and 12 ppm, respectively. The number of scans per t_1 increment was 16. 2D ^{1}H-^{1}H TOCSY spectra of *Arabidopsis thailana* metabolite extract were collected with N1=512 and N2=1024 complex points. The spectral widths along the indirect and direct dimension were 12 ppm and TOCSY mixing time was 90 ms. 2D spectra (including ^{1}H-^{13}C heteronuclear single-quantum correlation spectroscopy (HSQC),^{1}H-^{1}H total correlation spectroscopy (TOCSY)) were acquired on most of the leaf extract samples, aiding as needed in the 1D ^{1}H assignments.

Gas chromatography-mass spectrometry (GC-MS) based untargeted analysis of extracted metabolites was following Xu and colleagues [127]. The polar metabolites were completely dried under speed vacuum concentrator, then, chemically derivatized and analyzed by GC-MS. Metabolites were derivatized as previously described [128] by adding 20 µl of methoxyamine solution (30 mg/ml in pyridine) and incubated at 37 °C for 90 mins. to protect the carbonyl groups and reduce carbohydrate isoforms. Then 80 µl of N-methyl-N-(trimethylsilyl)-trifluoroacetamide with 1% trimethylchlorosilane were added to each sample to trimethylsilyate the hydroxyl and amine groups for 30 mins. The samples were cooled to room temperature prior to GC-MS analysis. Data collected by GC-MS were

processed using the MetaboliteDetector software, version 2.5 beta [129]. Retention indices of detected metabolites were calculated based on analysis of the fatty acid methyl esters mixture (C8 - C28), followed by chromatographic alignment across all analyses after deconvolution. Metabolites were initially identified by matching experimental spectra to a PNNL augmented version of the Agilent Fiehn Metabolomics Library containing spectra and validated retention indices for over 900 metabolites [130], and additionally cross-checked by matching with NIST17 GC-MS Spectral Library. All metabolite identifications were manually validated to minimize deconvolution and identification errors during the automated data processing.

The NMR and GCMS datasets were conducted on separate experimental replicates, which displayed variation in their overall responses that we attributed to effect of replicate. To account for this, we analyzed only those metabolites in common between the two datasets (**Table S3**), first transforming the data using centered-log ratio [51,52], then using Analysis of Variance (ANOVA, function *aov* in R v. 4.1.1) considering the effects of genotype, [CO_2], their interaction, and experimental replicate as a covariate. Each metabolite was analyzed separately, then the *p*-values adjusted for multiple comparisons using the *p.adjust* function in base R (v. 4.1.1, method = fdr) [131]. *Post hoc* analysis through Tukey's Honest Significant Difference (function *TukeyHSD*, v. 4.1.1), was used to assess differences among treatment groups.

Transcriptomic Profiling

a. Assembly of the SG and CG genomes

RNAseq and related bioinformatics were conducted in partnership with EMSL utilizing reference genomes for SG and CG sequenced through the University of Kansas Genomics CORE facility. Genomic DNA isolation, library preparation, and sequencing were as previously described [50]. Specifically, genomic DNA was isolated using the DNeasy Plant kit (Qiagen, Denmark) from two pooled, fully inbred plants from both the CG and SG lines. The libraries were prepared using the TruSeq DNA PCR-Free kit and sequenced on the HiSeq RR-PE100 system (Illumina, USA). This resulted in approximately 188 million reads in total or about 94 million reads per pooled sample, and about 200x coverage. These 100-bp reads were assembled into genes-only CG and SG genomes using ABySS assembly software (version 1.9.0, doi: 10.1101/gr.214346.116) using K=96. To predict the location of genes on the assembled sequences, we used the gene calling web server Augustus (http://bioinf.unigreifswald.de/augustus/submission.php). For each sequence predicted to be a gene, gene annotation was acquired using the best hit from a BLASTP search, using the plant component of Uniprot combined with the Araport11 gene set (https://www.araport.org/data/araport11). Genes received a genome specific identifier, as well as were matched with their most closely corresponding locus-linked *Arabidopsis* gene ID.

b. RNA sequencing

RNA was isolated using Qiagen RNeasy™ mini kit (cat#74104), followed by genomic DNA removal and cleaning using Qiagen RNase-Free DNase Set kit (cat#79254) and Qiagen Mini RNeasy™ kit (cat#74104) (Qiagen, Denmark). Integrity of the RNA samples was assessed using the Alegient 2100 Bioanalyzer. RNA samples having an RNA Integrity Number between nine and ten were used in this work. rRNA was removed using Ribo-Zero rRNA removal kit (cat#MRRZPL1224, Illumina, San Diego, CA, USA). The SOLiD™ Total RNA-Seq Kit

(cat#4445374) was used to construct template cDNA for RNASeq following the whole transcriptome protocol recommended by Applied Biosystems. Briefly, mRNA was fragmented using chemical hydrolysis followed by ligation with strand-specific adapters and reverse transcript to generate cDNA. The cDNA fragments, 150 to 250 bp in size, were isolated and amplified through 15 amplification cycles to produce the required number of templates for the SOLiD™ EZ Bead™ system, which was used to generate the strand-specific template bead library for ligation base sequencing by the 5500xl SOLiD™ instrument (LifeTechnologies, ThermoFisher, Carlsbad, CA, USA). The 50-base short read sequences produced by the SOLiD sequencer were mapped in color space using the Whole Transcriptome analysis pipeline in the Life Technologies LifeScope software version 2.5 against the genes-only genomes assembled, as described above, for the CG and SG Arabidopsis strains as well as the Araport11 reference genome.

c. Transcriptome analysis

Alignments to genotype-specific and Araport11 reference genomes were compared, and the Araport11 alignments were selected for continued use, as read count was higher. Specifically, count datasets for individual samples were compiled into a single dataset using R (v. 3.6.3), and rows containing duplicate gene identifiers were averaged for each individual as counts were similar or the same across rows containing the same gene identifiers (using the *aggregate* function in R). This resulted in 31,556 unique transcript identifiers. Individuals and counts were assessed for quality using the *goodSamplesGenes* function in the *WGCNA* package in R (v. 3.6.3, minFraction = ¾), then transcript identifiers containing mostly zeros were removed using the *count_filter* function in the *ERSSA* package in R (v. 3.6.3, cutoff = 1). This resulted in 16,472 unique transcript identifiers.

These remaining counts were analyzed using a workflow previously suggested for compositional data (i.e. data for which the upper bounds are limited by detection method and thus not representative of the true high values) [51,52]. Through this method, counts within a sample are relativized against the centered log ratio (clr) of all transcripts within a sample. To do so, any remaining zeros were replaced with very low values using the *cmultRep1* function in the *zCompositions* package in R (v. 4.1.1), then the clr was calculated for each transcript identifier and sample using the *clr* function in the *rgr* package in R (v. 4.1.1). These relativized values were used to calculate the Aitchison distances among samples using the *dist* function in the *robCompositions* package in R (v. 4.1.1, method = euclidean). Samples were clustered based on these distances using the *hclust* function, and two samples, one in CG and one in SG were determined to be outliers as they grouped together, but independently of all other samples in each genotype (**Fig. S1**). These samples were removed, then the distances recalculated. The Aitchison distances were then used to explore relationships among samples and across genotype and [CO_2] treatments using Principal Component Analysis (PCA, *prcomp* function in R) and multivariate comparison using the *adonis* function in the *vegan* package in R (v. 4.1.1), which allows for interactions among treatments. Once these broad patterns among samples were determined, differential expression analysis of independent transcript identifiers was conducted across genotypes and [CO_2] treatments (*aldex.clr* function, *ALDEx2* package), and across [CO_2] treatments within each genotype separately (*aldex* function, *ALDEx2* package). Transcript identifiers with effect sizes greater than ±1 [52] were pulled out for functional annotation analysis using DAVID and the functional annotation clustering function

(david.ncifcrf.gov) [132,133], which pulls annotation terms from multiple resources and clusters those terms based on the overlap in genes used to call each term. Clusters with p values of 0.05 were considered significant. A list of 156 flowering regulator genes, of which 125 corresponded to the transcript identifiers in this dataset, were analyzed separately for effect sizes calculated between [CO_2] within a genotype using the following: $(\mu_1 - \mu_2)/\text{mean}(\sigma_1, \sigma_2)$, where μ and σ are the group mean and standard deviation for a transcript identifier across a treatment group.

Data availability statement

Raw data and codes for analysis will be made available on Open Science Framework at the time of publication. View-only link for review: https://osf.io/zbdq2/?view_only=a117caf2d2e74bc28a3442bba742080c

Acknowledgements

The authors thank Aleah Henderson-Carter for her help in maintaining and conducting the experiments, Dr. Lena Hileman for her ongoing encouragement, and Drs. John Kelly, Maggie Wagner, and the participants of EEB Genetics for their helpful advice in the analysis. We also thank the University of Kansas Genome Core Facility for their role in this work and their technical support. This work was supported by National Science Foundation (IOS-1457236) to JKW, and the National Institute of Health Research and Academic Career Development Award (IRADCA) fellowship K12GM063651 to HK-S. A portion of this research was performed on a project award (10.46936/sthm.proj.2013.47814/60005186) from the Environmental Molecular Sciences Laboratory, a Department of Energy Office of Science User Facility sponsored by the Biological and Environmental Research program under Contract No. DE-AC05-76RL01830. Pacific Northwest National Laboratory is a multi-program national laboratory operated by Battelle for the Department of Energy under Contract No. DE-AC05-76RLO1830. The funders has no role in study design, data collection and analysis, decision to publish, or preparation of the manuscript.

References

1. Masson-Delmotte V, Zhai P, Pirani A, Connors SL, Péan C, Berger S, Caud N, Chen Y, Goldfarb L, Gomis MI, Huang M, Leitzell K, Lonnoy E, Matthews JBR, Maycock TK, Waterfield T, Yelekçi Ö, Yu R, Zhou B, editors. Climate Change 2021: The Physical Science Basis. Contribution of Working Group I to the Sixth Assessment Report of the Intergovernmental Panel on Climate Change. Cambridge University Press; 2021.

2. Inouye DW. Effects of Climate Change on Phenology, Frost Damage, and Floral Abundance of Montane Wildflowers. Ecology. 2008;89(2):353–62.

3. Rafferty NE, Ives AR. Pollinator effectiveness varies with experimental shifts in flowering time. Ecology. 2012 Apr;93(4):803–14.

4. Schmidt NM, Mosbacher JB, Nielsen PS, Rasmussen C, Høye TT, Roslin T. An ecological function in crisis? The temporal overlap between plant flowering and pollinator function shrinks as the Arctic warms. Ecography. 2016 Dec;39(12):1250–2.

678 5. Forrest JRK. Plant–pollinator interactions and phenological change: what can we learn
679 about climate impacts from experiments and observations? Oikos. 2015;124(1):4–13.

680 6. Miller-Struttmann NE, Geib JC, Franklin JD, Kevan PG, Holdo RM, Ebert-May D, Lynn AM,
681 Kettenbach JA, Hedrick E, Galen C. Functional mismatch in a bumble bee pollination
682 mutualism under climate change. Science. 2015 Sep 25;349(6255):1541–4.

683 7. Bartomeus I, Park MG, Gibbs J, Danforth BN, Lakso AN, Winfree R. Biodiversity ensures
684 plant–pollinator phenological synchrony against climate change. Ecology Letters.
685 2013;16(11):1331–8.

686 8. Cui T, Martz L, Guo X. Grassland Phenology Response to Drought in the Canadian Prairies.
687 Remote Sensing. 2017 Dec;9(12):1258.

688 9. Bernal M, Estiarte M, Peñuelas J. Drought advances spring growth phenology of the
689 Mediterranean shrub Erica multiflora. Plant Biology. 2011;13(2):252–7.

690 10. Ma Q, Huang JG, Hänninen H, Berninger F. Divergent trends in the risk of spring frost
691 damage to trees in Europe with recent warming. Global Change Biology. 2019;25(1):351–
692 60.

693 11. Franks SJ, Sim S, Weis AE. Rapid evolution of flowering time by an annual plant in response
694 to a climate fluctuation. Proceedings of the National Academy of Sciences. 2007 Jan
695 23;104(4):1278–82.

696 12. Walker SM, Ward JK. Interactions between rising CO<Subscript>2</Subscript> and
697 temperature drive accelerated flowering in model plants under changing conditions of the
698 last century. Oecologia. 2018 Aug 1;187(4):911–9.

699 13. Springer CJ, Ward JK. Flowering time and elevated atmospheric CO_2. New Phytologist.
700 2007;176(2):243–55.

701 14. Ward JK, Antonovics J, Thomas RB, Strain BR. Is atmospheric CO<Subscript>2</Subscript>
702 a selective agent on model C-3 annuals? Oecologia. 2000 May;123(3):330–41.

703 15. Springer CJ, Orozco RA, Kelly JK, Ward JK. Elevated CO_2 influences the expression of floral-
704 initiation genes in *Arabidopsis thaliana*. New Phytol. 2008;178(1):63–7.

705 16. Bunce JA, Hilacondo WC. Responses of Flowering Time to Elevated Carbon Dioxide among
706 Soybean Photoperiod Isolines. American Journal of Plant Sciences. 2016 Apr 5;7(6):773–9.

707 17. Misra BB, Chen S. Advances in understanding CO_2 responsive plant metabolomes in the
708 era of climate change. Metabolomics. 2015 Dec 1;11(6):1478–91.

709 18. Evans LT, Wardlaw IF. Independent translocation of 14C-labelled assimilates and of the
710 floral stimulus in Lolium temulentum. Planta. 1966 Dec 1;68(4):310–26.

19. Bodson M, King R, Evans L, Bernier G. The Role of Photosynthesis in Flowering of the Long-Day Plant *Sinapis alba*. Functional Plant Biol. 1977 Jan 1;4(4):467–78.

20. Perilleux C, Bernier G. Leaf carbohydrate status in Lolium temulentum during the induction of flowering. New Phytol. 1997 Jan;135(1):59–66.

21. Lejeune P, Bernier G, Requier MC, Kinet JM. Sucrose increase during floral induction in the phloem sap collected at the apical part of the shoot of the long-day plant *Sinapis alba* L. Planta. 1993 May 1;190(1):71–4.

22. Corbesier L, Bernier G, Perilleux C. C : N Ratio Increases in the Phloem Sap During Floral Transition of the Long-Day Plants *Sinapis alba* and *Arabidopsis thaliana*. Plant Cell Physiology. 2002;43(6):684–8.

23. Corbesier L, Lejeune P, Bernier G. The role of carbohydrates in the induction of flowering in *Arabidopsis thaliana*: comparison between the wild type and a starchless mutant. Planta. 1998;206(1):131–7.

24. Ohto M, Onai K, Furukawa Y, Aoki E, Araki T, Nakamura K. Effects of sugar on vegetative development and floral transition in *Arabidopsis*. Plant Physiol. 2001 Sep;127(1):252–61.

25. Wahl V, Ponnu J, Schlereth A, Arrivault S, Langenecker T, Franke A, Feil R, Lunn JE, Stitt M, Schmid M. Regulation of flowering by trehalose-6-phosphate signaling in *Arabidopsis thaliana*. - PubMed - NCBI. Science. 2013;339(6120):704–7.

26. Hanover JA, Krause MW, Love DC. Bittersweet memories: linking metabolism to epigenetics through O-GlcNAcylation. Nat Rev Mol Cell Biol. 2012 May;13(5):312–21.

27. Xu SL, Chalkley RJ, Maynard JC, Wang W, Ni W, Jiang X, Shin K, Cheng L, Savage D, Hühmer AFR, Burlingame AL, Wang ZY. Proteomic analysis reveals O-GlcNAc modification on proteins with key regulatory functions in *Arabidopsis*. Proc Natl Acad Sci U S A. 2017 Feb 21;114(8):E1536–43.

28. Hardivillé S, Hart GW. Nutrient Regulation of Signaling, Transcription, and Cell Physiology by O-GlcNAcylation. Cell Metabolism. 2014 Aug 5;20(2):208–13.

29. Kawai T, Yamada T, Abe K, Okamura K, Kamura H, Akaishi R, Minakami H, Nakabayashi K, Hata K. Increased epigenetic alterations at the promoters of transcriptional regulators following inadequate maternal gestational weight gain. Sci Rep. 2015 Sep 29;5:14224.

30. Zentella R, Hu J, Hsieh WP, Matsumoto PA, Dawdy A, Barnhill B, Oldenhof H, Hartweck LM, Maitra S, Thomas SG, Cockrell S, Boyce M, Shabanowitz J, Hunt DF, Olszewski NE, Sun T ping. O-GlcNAcylation of master growth repressor DELLA by SECRET AGENT modulates multiple signaling pathways in *Arabidopsis*. Genes Dev. 2016 Jan 15;30(2):164–76.

31. Xing L, Liu Y, Xu S, Xiao J, Wang B, Deng H, Lu Z, Xu Y, Chong K. *Arabidopsis* O-GlcNAc transferase SEC activates histone methyltransferase ATX1 to regulate flowering. The EMBO Journal. 2018 Aug 27;e98115.

32. Claeys H, Inzé D. The Agony of Choice: How Plants Balance Growth and Survival under Water-Limiting Conditions. Plant Physiol. 2013 Aug 1;162(4):1768–79.

33. Ljung K, Nemhauser JL, Perata P. New mechanistic links between sugar and hormone signalling networks. Curr Opin Plant Biol. 2015 Jun;25:130–7.

34. Pyo Y, Park S, Xi Y, Sung S. Regulation of flowering by vernalisation in *Arabidopsis*. Advances in Botanical Research. 2014;72:29–61.

35. Locasale JW. Serine, glycine and one-carbon units: cancer metabolism in full circle. Nature Reviews Cancer. 2013 Aug;13(8):572–83.

36. Janke R, Dodson AE, Rine J. Metabolism and Epigenetics. Annual Review of Cell and Developmental Biology. 2015;31(1):473–96.

37. Ros R, Muñoz-Bertomeu J, Krueger S. Serine in plants: biosynthesis, metabolism, and functions. Trends in Plant Science. 2014 Sep 1;19(9):564–9.

38. El-Lithy ME, Reymond M, Stich B, Koornneef M, Vreugdenhil D. Relation among plant growth, carbohydrates and flowering time in the Arabidopsis Landsberg erecta × Kondara recombinant inbred line population. Plant, Cell & Environment. 2010;33(8):1369–82.

39. Cross JM, von Korff M, Altmann T, Bartzetko L, Sulpice R, Gibon Y, Palacios N, Stitt M. Variation of Enzyme Activities and Metabolite Levels in 24 Arabidopsis Accessions Growing in Carbon-Limited Conditions. Plant Physiology. 2006 Dec 1;142(4):1574–88.

40. Ursi S, Pedersén M, Plastino E, Snoeijs P. Intraspecific variation of photosynthesis, respiration and photoprotective carotenoids in Gracilaria birdiae (Gracilariales: Rhodophyta). Marine Biology. 2003 May 1;142(5):997–1007.

41. Faralli M, Lawson T. Natural genetic variation in photosynthesis: an untapped resource to increase crop yield potential? The Plant Journal. 2020;101(3):518–28.

42. Ziska LH, Teramura AH. Intraspecific variation in the response of rice (Oryza sativa) to increased CO2– photosynthetic, biomass and reproductive characteristics. Physiologia Plantarum. 1992;84(2):269–74.

43. Thilakarathne CL, Tausz-Posch S, Cane K, Norton RM, Tausz M, Seneweera S, Thilakarathne CL, Tausz-Posch S, Cane K, Norton RM, Tausz M, Seneweera S. Intraspecific variation in growth and yield response to elevated CO2 in wheat depends on the differences of leaf mass per unit area. Functional Plant Biol. 2012 Sep 17;40(2):185–94.

44. Stéphanie Arrivault, Thiago Alexandre Moraes, Toshihiro Obata, David B Medeiros, Alisdair R Fernie, Alix Boulouis, Martha Ludwig, John E Lunn, Gian Luca Borghi, Armin Schlereth, Manuela Guenther, Mark Stitt. Metabolite profiles reveal interspecific variation in operation of the Calvin–Benson cycle in both C_4 and C_3 plants. Journal of experimental botany. 2019 Mar 27;70(6):1843–58.

45. Van Der Kooij TAW, De Kok LJ, Stulen I. Intraspecific Variation in the Response if *Arabidopsis thaliana* Lines to Elevated Atomospheric CO_2. Phyton; Annales Rei Botanicae. 2000 Mar 31;40(3):125–32.

46. Capovilla G, Schmid M, Pose D. Control of flowering by ambient temperature. J Exp Bot. 2015 Jan;66(1):59–69.

47. Lorenzo CD, Sanchez-Lamas M, Antonietti MS, Cerdán PD. Emerging Hubs in Plant Light and Temperature Signaling. Photochemistry and Photobiology. 2016;92(1):3–13.

48. Song YH, Ito S, Imaizumi T. Flowering time regulation: photoperiod- and temperature-sensing in leaves. Trends Plant Sci. 2013 Oct;18(10):575–83.

49. Searle I, He Y, Turck F, Vincent C, Fornara F, Kröber S, Amasino RA, Coupland G. The transcription factor FLC confers a flowering response to vernalization by repressing meristem competence and systemic signaling in *Arabidopsis*. Genes Dev. 2006 Apr 1;20(7):898–912.

50. Henderson-Carter AL, Kinmonth-Schultz H, Hileman L, Ward JK. *FLOWERING LOCUS C* drives delayed flowering in *Arabidopsis* grown and selected at elevated CO_2. bioRxiv [Internet]. 2023 Jun 15;2023.06.15.545149. Available from: https://www.biorxiv.org/content/10.1101/2023.06.15.545149v1

51. Quinn TP, Erb I, Gloor G, Notredame C, Richardson MF, Crowley TM. A field guide for the compositional analysis of any-omics data. GigaScience [Internet]. 2019 Sep 1 [cited 2021 Sep 21];8(9). Available from: https://doi.org/10.1093/gigascience/giz107

52. Gloor GB, Macklaim JM, Pawlowsky-Glahn V, Egozcue JJ. Microbiome Datasets Are Compositional: And This Is Not Optional. Frontiers in Microbiology. 2017;8:2224.

53. Aitchison J. The Statistical Analysis of Compositional Data. Journal of the Royal Statistical Society: Series B (Methodological). 1982;44(2):139–60.

54. Hymus GJ, Baker NR, Long SP. Growth in Elevated CO2 Can Both Increase and Decrease Photochemistry and Photoinhibition of Photosynthesis in a Predictable Manner. Dactylis glomerata Grown in Two Levels of Nitrogen Nutrition. Plant Physiology. 2001 Nov 1;127(3):1204–11.

55. Rasineni GK, Guha A, Reddy AR. Elevated atmospheric CO2 mitigated photoinhibition in a tropical tree species, Gmelina arborea. Journal of Photochemistry and Photobiology B: Biology. 2011 May 3;103(2):159–65.

56. Berardini TZ, Reiser L, Li D, Mezheritsky Y, Muller R, Strait E, Huala E. TAIR. The Arabidopsis Information Resource: Making and mining the "gold standard" annotated reference plant genome. genesis [Internet]. 2015; Available from: https://www.arabidopsis.org/doc/about/tair_terms_of_use/417

57. Loizeau K, Gambonnet B, Zhang GF, Curien G, Jabrin S, Van Der Straeten D, Lambert WE, Rebeille F, Ravanel S. Regulation of one-carbon metabolism in arabidopsis: The N-terminal regulatory domain of cystathionine gamma-synthase is cleaved in response to folate starvation. Plant Physiol. 2007 Oct;145(2):491–503.

58. Tamada Y, Yun JY, Woo SC, Amasino RM. ARABIDOPSIS TRITHORAX-RELATED7 is required for methylation of lysine 4 of histone H3 and for transcriptional activation of FLOWERING LOCUS C. Plant Cell. 2009;21:3257–69.

59. Ravanel S, Douce R, Rébeillé F. The Uniqueness of Tetrahydrofolate Synthesis and One-Carbon Metabolism in Plants. In: Day DA, Millar AH, Whelan J, editors. Plant Mitochondria: From Genome to Function [Internet]. Dordrecht: Springer Netherlands; 2004 [cited 2021 Jul 2]. p. 277–92. (Advances in Photosynthesis and Respiration). Available from: https://doi.org/10.1007/978-1-4020-2400-9_12

60. Figueroa CM, Lunn JE. A Tale of Two Sugars: Trehalose 6-Phosphate and Sucrose. Plant Physiol. 2016 Sep 1;172(1):7–27.

61. van Dijken AJH, Schluepmann H, Smeekens SCM. Arabidopsis trehalose-6-phosphate synthase 1 is essential for normal vegetative growth and transition to flowering. Plant Physiol. 2004 Jun;135(2):969–77.

62. Baena-González E, Lunn JE. SnRK1 and trehalose 6-phosphate – two ancient pathways converge to regulate plant metabolism and growth. Current Opinion in Plant Biology. 2020 Jun 1;55:52–9.

63. Jeong EY, Seo PJ, Woo JC, Park CM. AKIN10 delays flowering by inactivating IDD8 transcription factor through protein phosphorylation in *Arabidopsis*. BMC Plant Biol. 2015 May 1;15:110.

64. Fragoso S, Espíndola L, Páez-Valencia J, Gamboa A, Camacho Y, Martínez-Barajas E, Coello P. SnRK1 Isoforms AKIN10 and AKIN11 Are Differentially Regulated in Arabidopsis Plants under Phosphate Starvation. Plant Physiology. 2009 Apr;149(4):1906.

65. Sun TP. Novel nucleocytoplasmic protein O-fucosylation by SPINDLY regulates diverse developmental processes in plants. Curr Opin Struct Biol. 2021 Jun;68:113–21.

66. Hartweck LM, Scott CL, Olszewski NE. Two O-Linked N-Acetylglucosamine Transferase Genes of Arabidopsis thaliana L. Heynh. Have Overlapping Functions Necessary for Gamete and Seed Development. Genetics. 2002 Jul 1;161(3):1279–91.

67. Zentella R, Sui N, Barnhill B, Hsieh WP, Hu J, Shabanowitz J, Boyce M, Olszewski NE, Zhou P, Hunt DF, Sun T ping. The Arabidopsis O-fucosyltransferase SPINDLY activates nuclear growth repressor DELLA. Nat Chem Biol. 2017 May;13(5):479–85.

68. Bouché F, Lobet G, Tocquin P, Périlleux C. FLOR-ID: an interactive database of flowering-time gene networks in *Arabidopsis thaliana*. Nucleic Acids Research. 2016 Jan 4;44(D1):D1167–71.

69. Jiang D, Kong NC, Gu X, Li Z, He Y. Arabidopsis COMPASS-Like Complexes Mediate Histone H3 Lysine-4 Trimethylation to Control Floral Transition and Plant Development. PLOS Genetics. 2011 Mar 10;7(3):e1001330.

70. Choi K, Kim J, Hwang HJ, Kim S, Park C, Kim SY, Lee I. The FRIGIDA Complex Activates Transcription of *FLC*, a Strong Flowering Repressor in *Arabidopsis*, by Recruiting Chromatin Modification Factors. The Plant Cell. 2011 Jan 1;23(1):289–303.

71. Kobayashi Y, Weigel D. Move on up, it's time for change--mobile signals controlling photoperiod-dependent flowering. Genes Dev. 2007 Oct 1;21(19):2371–84.

72. Lee J, Oh M, Park H, Lee I. SOC1 translocated to the nucleus by interaction with AGL24 directly regulates *LEAFY*. Plant J. 2008;55(5):832–43.

73. Yamaguchi A, Wu MF, Yang L, Wu G, Poethig RS, Wagner D. The MicroRNA-Regulated SBP-Box Transcription Factor SPL3 Is a Direct Upstream Activator of LEAFY, FRUITFULL, and APETALA1. Developmental Cell. 2009 Aug 18;17(2):268–78.

74. Wang JW, Czech B, Weigel D. miR156-Regulated SPL Transcription Factors Define an Endogenous Flowering Pathway in Arabidopsis thaliana. Cell. 2009 Aug 21;138(4):738–49.

75. Zubo YO, Blakley IC, Franco-Zorrilla JM, Yamburenko MV, Solano R, Kieber JJ, Loraine AE, Schaller GE. Coordination of Chloroplast Development through the Action of the GNC and GLK Transcription Factor Families. Plant Physiology. 2018 Sep 1;178(1):130–47.

76. Klermund C, Ranftl QL, Diener J, Bastakis E, Richter R, Schwechheimer C. LLM-Domain B-GATA Transcription Factors Promote Stomatal Development Downstream of Light Signaling Pathways in Arabidopsis thaliana Hypocotyls. The Plant Cell. 2016 Mar 1;28(3):646–60.

77. Hudson D, Guevara D, Yaish MW, Hannam C, Long N, Clarke JD, Bi YM, Rothstein SJ. GNC and CGA1 Modulate Chlorophyll Biosynthesis and Glutamate Synthase (GLU1/Fd-GOGAT) Expression in Arabidopsis. PLOS ONE. 2011 Nov 10;6(11):e26765.

879 78. Bi YM, Zhang Y, Signorelli T, Zhao R, Zhu T, Rothstein S. Genetic analysis of Arabidopsis
880 GATA transcription factor gene family reveals a nitrate-inducible member important for
881 chlorophyll synthesis and glucose sensitivity. The Plant Journal. 2005;44(4):680–92.

882 79. Yang J, Xu Y, Wang J, Gao S, Huang Y, Hung FY, Li T, Li Q, Yue L, Wu K, Yang S. The
883 chromatin remodelling ATPase BRAHMA interacts with GATA-family transcription factor
884 GNC to regulate flowering time in Arabidopsis. Journal of Experimental Botany. 2022 Jan
885 27;73(3):835–47.

886 80. Richter R, Bastakis E, Schwechheimer C. Cross-Repressive Interactions between SOC1 and
887 the GATAs GNC and GNL/CGA1 in the Control of Greening, Cold Tolerance, and Flowering
888 Time in Arabidopsis. Plant Physiology. 2013 Aug 1;162(4):1992–2004.

889 81. Somers DE, Webb AA, Pearson M, Kay SA. The short-period mutant, toc1-1, alters
890 circadian clock regulation of multiple outputs throughout development in Arabidopsis
891 thaliana. Development. 1998 Feb;125(3):485–94.

892 82. Sawa M, Nusinow DA, Kay SA, Imaizumi T. FKF1 and GIGANTEA complex formation is
893 required for day-length measurement in *Arabidopsis*. Science. 2007 Oct
894 12;318(5848):261–5.

895 83. Fowler S, Lee K, Onouchi H, Samach A, Richardson K, Morris B, Coupland G, Putterill J.
896 GIGANTEA: a circadian clock-controlled gene that regulates photoperiodic flowering in
897 Arabidopsis and encodes a protein with several possible membrane-spanning domains.
898 EMBO J. 1999 Sep 1;18(17):4679–88.

899 84. Bläsing OE, Gibon Y, Günther M, Höhne M, Morcuende R, Osuna D, Thimm O, Usadel B,
900 Scheible WR, Stitt M. Sugars and Circadian Regulation Make Major Contributions to the
901 Global Regulation of Diurnal Gene Expression in Arabidopsis. The Plant Cell. 2005 Dec
902 1;17(12):3257–81.

903 85. Graf A, Schlereth A, Stitt M, Smith AM. Circadian control of carbohydrate availability for
904 growth in Arabidopsis plants at night. PNAS [Internet]. 2010 May 3 [cited 2012 Aug 9];
905 Available from: http://www.pnas.org/content/early/2010/04/21/0914299107

906 86. Haydon MJ, Mielczarek O, Robertson FC, Hubbard KE, Webb AAR. Photosynthetic
907 entrainment of the *Arabidopsis thaliana* circadian clock. Nature. 2013 Oct
908 31;502(7473):689–92.

909 87. Shin J, Sánchez-Villarreal A, Davis AM, Du S xiu, Berendzen KW, Koncz C, Ding Z, Li C, Davis
910 SJ. The metabolic sensor AKIN10 modulates the Arabidopsis circadian clock in a light-
911 dependent manner. Plant, Cell & Environment. 2017;40(7):997–1008.

912 88. Imaizumi T, Schultz TF, Harmon FG, Ho LA, Kay SA. FKF1 F-box protein mediates cyclic
913 degradation of a repressor of CONSTANS in *Arabidopsis* . Science. 2005;309:293–7.

89. Samach A, Onouchi H, Gold SE, Ditta GS, Schwarz-Sommer Z, Yanofsky MF, Coupland G. Distinct roles of CONSTANS target genes in reproductive development of *Arabidopsis*. Science. 2000 Jun 2;288(5471):1613–6.

90. Valverde F, Mouradov A, Soppe W, Ravenscroft D, Samach A, Coupland G. Photoreceptor regulation of CONSTANS protein in photoperiodic flowering. Science. 2004;303:1003–6.

91. Jang S, Marchal V, Panigrahi KCS, Wenkel S, Soppe W, Deng XW, Valverde F, Coupland G. *Arabidopsis* COP1 shapes the temporal pattern of CO accumulation conferring a photoperiodic flowering response. EMBO J. 2008 Apr 23;27(8):1277–88.

92. Laubinger S, Marchal V, Le Gourrierec J, Gentilhomme J, Wenkel S, Adrian J, Jang S, Kulajta C, Braun H, Coupland G, Hoecker U. *Arabidopsis* SPA proteins regulate photoperiodic flowering and interact with the floral inducer CONSTANS to regulate its stability. Development. 2006 Aug;133(16):3213–22.

93. Laubinger S, Hoecker U. The SPA1-like proteins SPA3 and SPA4 repress photomorphogenesis in the light. Plant Journal. 2003;35:373–85.

94. Saijo Y, Sullivan JA, Wang H, Yang J, Shen Y, Rubio V, Ma L, Hoecker U, Deng XW. The COP1-SPA1 interaction defines a critical step in phytochrome A-mediated regulation of HY5 activity. Genes Dev. 2003;17:2642–7.

95. Nguyen KT, Park J, Park E, Lee I, Choi G. The Arabidopsis RING Domain Protein BOI Inhibits Flowering via CO-dependent and CO-independent Mechanisms. Molecular Plant. 2015 Dec 7;8(12):1725–36.

96. Castillejo C, Pelaz S. The balance between CONSTANS and TEMPRANILLO activities determines FT expression to trigger flowering. Curr Biol. 2008;18:1338–43.

97. Hu H, Tian S, Xie G, Liu R, Wang N, Li S, He Y, Du J. TEM1 combinatorially binds to FLOWERING LOCUS T and recruits a Polycomb factor to repress the floral transition in Arabidopsis. Proc Natl Acad Sci U S A. 2021 Aug 31;118(35):e2103895118.

98. Park J, Nguyen KT, Park E, Jeon JS, Choi G. DELLA Proteins and Their Interacting RING Finger Proteins Repress Gibberellin Responses by Binding to the Promoters of a Subset of Gibberellin-Responsive Genes in Arabidopsis. The Plant Cell. 2013 Mar 1;25(3):927–43.

99. Osnato M, Castillejo C, Matías-Hernández L, Pelaz S. TEMPRANILLO genes link photoperiod and gibberellin pathways to control flowering in Arabidopsis. Nat Commun. 2012 May 1;3(1):808.

100. Matsoukas IG. Interplay between sugar and hormone signaling pathways modulate floral signal transduction. Frontiers in Genetics [Internet]. 2014 [cited 2022 Mar 7];5. Available from: https://www.frontiersin.org/article/10.3389/fgene.2014.00218

101. Earley EJ, Ingland B, Winkler J, Tonsor SJ. Inflorescences contribute more than rosettes to lifetime carbon gain in Arabidopsis thaliana (Brassicaceae). Am J Bot. 2009 Apr 1;96(4):786–92.

102. Adams WWI, Stewart JJ, Cohu CM, Muller O, Demmig-Adams B. Habitat Temperature and Precipitation of Arabidopsis thaliana Ecotypes Determine the Response of Foliar Vasculature, Photosynthesis, and Transpiration to Growth Temperature. Front Plant Sci [Internet]. 2016 [cited 2020 Mar 24];7. Available from: https://www.frontiersin.org/articles/10.3389/fpls.2016.01026/full

103. De Coninck T, Gistelinck K, Janse van Rensburg HC, Van den Ende W, Van Damme EJM. *Sweet Modifications Modulate Plant Development. Biomolecules. 2021 May 18;11(5):756.

104. Love DC, Krause MW, Hanover JA. O-GlcNAc cycling: Emerging Roles in Development and Epigenetics. Semin Cell Dev Biol. 2010 Aug;21(6):646–54.

105. Waalen WM, Stavang JA, Olsen JE, Rognli OA. The relationship between vernalization saturation and the maintenance of freezing tolerance in winter rapeseed. Environmental and Experimental Botany. 2014 Oct 1;106:164–73.

106. Klotke J, Kopka J, Gatzke N, Heyer AG. Impact of soluble sugar concentrations on the acquisition of freezing tolerance in accessions of *Arabidopsis thaliana* with contrasting cold adaptation – evidence for a role of raffinose in cold acclimation. Plant, Cell & Environment. 2004;27(11):1395–404.

107. Joudi M, Ahmadi A, Mohamadi V, Abbasi A, Vergauwen R, Mohammadi H, Van den Ende W. Comparison of fructan dynamics in two wheat cultivars with different capacities of accumulation and remobilization under drought stress. Physiologia Plantarum. 2012;144(1):1–12.

108. Mitchell PJ, O'Grady AP, Tissue DT, White DA, Ottenschlaeger ML, Pinkard EA. Drought response strategies define the relative contributions of hydraulic dysfunction and carbohydrate depletion during tree mortality. New Phytologist. 2013;197(3):862–72.

109. Kafi M, Stewart WS, Borland AM. Carbohydrate and Proline Contents in Leaves, Roots, and Apices of Salt-Tolerant and Salt-Sensitive Wheat Cultivars1. Russian Journal of Plant Physiology. 2003 Mar 1;50(2):155–62.

110. Kerepesi I, Galiba G. Osmotic and Salt Stresses Induced Differential Alteration in Water-Soluble Carbohydrate Content in Wheat Seedlings. J Agric Food Chem. 1998 Dec 1;46(12):5347–54.

111. Kinmonth-Schultz H, Kim SH. Carbon gain, allocation and storage in rhizomes in response to elevated atmospheric carbon dioxide and nutrient supply in a perennial C3 grass, *Phalaris arundinacea*. Funct Plant Biol. 2011;38(10):797–807.

112. Liu J, Wang L, Wang D, Bonser SP, Sun F, Zhou Y, Gao Y, Teng X. Plants Can Benefit from Herbivory: Stimulatory Effects of Sheep Saliva on Growth of Leymus chinensis. PLOS ONE. 2012 Jan 3;7(1):e29259.

113. Pien S, Fleury D, Mylne JS, Crevillen P, Inzé D, Avramova Z, Dean C, Grossniklaus U. ARABIDOPSIS TRITHORAX1 Dynamically Regulates FLOWERING LOCUS C Activation via Histone 3 Lysine 4 Trimethylation. The Plant Cell. 2008 Mar 1;20(3):580–8.

114. Saleh A, Alvarez-Venegas R, Yilmaz M, Oahn-Le, Hou G, Sadder M, Al-Abdallat A, Xia Y, Lu G, Ladunga I, Avramova Z. The Highly Similar Arabidopsis Homologs of Trithorax ATX1 and ATX2 Encode Proteins with Divergent Biochemical Functions. Plant Cell. 2008 Mar;20(3):568–79.

115. Liu Y, Wang J, Yin H, Zhang A, Huang S, Wang TJ, Meng Q, Nan N, Wu Y, Guo P, Ahmad R, Liu B, Xu ZY. Trithorax-group protein ATX5 mediates the glucose response via impacting the HY1-ABI4 signaling module. Plant Mol Biol. 2018 Dec 1;98(6):495–506.

116. Ramon M, De Smet I, Vandesteene L, Naudts M, Leyman B, Van Dijck P, Rolland F, Beeckman T, Thevelein JM. Extensive expression regulation and lack of heterologous enzymatic activity of the Class II trehalose metabolism proteins from Arabidopsis thaliana. Plant Cell Environ. 2009 Aug;32(8):1015–32.

117. Paik I, Chen F, Ngoc Pham V, Zhu L, Kim JI, Huq E. A phyB-PIF1-SPA1 kinase regulatory complex promotes photomorphogenesis in Arabidopsis. Nat Commun. 2019 Sep 16;10(1):4216.

118. van der Laarse SAM, Leney AC, Heck AJR. Crosstalk between phosphorylation and O-GlcNAcylation: friend or foe. The FEBS Journal. 2018;285(17):3152–67.

119. Debrieux D, Trevisan M, Fankhauser C. Conditional Involvement of CONSTITUTIVE PHOTOMORPHOGENIC1 in the Degradation of Phytochrome A. Plant Physiology. 2013 Apr 1;161(4):2136–45.

120. Sheerin DJ, Menon C, zur Oven-Krockhaus S, Enderle B, Zhu L, Johnen P, Schleifenbaum F, Stierhof YD, Huq E, Hiltbrunner A. Light-Activated Phytochrome A and B Interact with Members of the SPA Family to Promote Photomorphogenesis in Arabidopsis by Reorganizing the COP1/SPA Complex. The Plant Cell. 2015 Jan 1;27(1):189–201.

121. Eriksson S, Böhlenius H, Moritz T, Nilsson O. GA4 Is the Active Gibberellin in the Regulation of LEAFY Transcription and Arabidopsis Floral Initiation. Plant Cell. 2006 Sep 1;18(9):2172–81.

122. Nohales MA, Kay SA. GIGANTEA gates gibberellin signaling through stabilization of the DELLA proteins in Arabidopsis. Proceedings of the National Academy of Sciences. 2019 Oct 22;116(43):21893–9.

123. Dalchau N, Baek SJ, Briggs HM, Robertson FC, Dodd AN, Gardner MJ, Stancombe MA, Haydon MJ, Stan GB, Gonçalves JM, Webb AAR. The circadian oscillator gene *GIGANTEA* mediates a long-term response of the *Arabidopsis thaliana* circadian clock to sucrose. PNAS. 2011 Mar 22;108(12):5104–9.

124. Ho SL, Huang LF, Lu CA, He SL, Wang CC, Yu SP, Chen J, Yu SM. Sugar starvation- and GA-inducible calcium-dependent protein kinase 1 feedback regulates GA biosynthesis and activates a 14-3-3 protein to confer drought tolerance in rice seedlings. Plant Mol Biol. 2013 Mar 1;81(4):347–61.

125. Ward JK, Strain BR. Effects of low and elevated CO_2 partial pressure on growth and reproduction of *Arabidopsis thaliana* from different elevations. Plant, Cell & Environment. 1997;20(2):254–60.

126. Weljie AM, Newton J, Mercier P, Carlson E, Slupsky CM. Targeted profiling: quantitative analysis of 1H NMR metabolomics data. Anal Chem. 2006 Jul 1;78(13):4430–42.

127. Xu L, Naylor D, Dong Z, Simmons T, Pierroz G, Hixson KK, Kim YM, Zink EM, Engbrecht KM, Wang Y, Gao C, DeGraaf S, Madera MA, Sievert JA, Hollingsworth J, Birdseye D, Scheller HV, Hutmacher R, Dahlberg J, Jansson C, Taylor JW, Lemaux PG, Coleman-Derr D. Drought delays development of the sorghum root microbiome and enriches for monoderm bacteria. Proceedings of the National Academy of Sciences. 2018 May;115(18):E4284–93.

128. Kim YM, Nowack S, Olsen MT, Becraft ED, Wood JM, Thiel V, Klapper I, Kühl M, Fredrickson JK, Bryant DA, Ward DM, Metz TO. Diel metabolomics analysis of a hot spring chlorophototrophic microbial mat leads to new hypotheses of community member metabolisms. Frontiers in Microbiology [Internet]. 2015 [cited 2022 Aug 10];6. Available from: https://www.frontiersin.org/articles/10.3389/fmicb.2015.00209

129. Hiller K, Hangebrauk J, Jäger C, Spura J, Schreiber K, Schomburg D. MetaboliteDetector: Comprehensive Analysis Tool for Targeted and Nontargeted GC/MS Based Metabolome Analysis. Anal Chem. 2009 May 1;81(9):3429–39.

130. Kind T, Wohlgemuth G, Lee DY, Lu Y, Palazoglu M, Shahbaz S, Fiehn O. FiehnLib: Mass Spectral and Retention Index Libraries for Metabolomics Based on Quadrupole and Time-of-Flight Gas Chromatography/Mass Spectrometry. Anal Chem. 2009 Dec 15;81(24):10038–48.

131. Jafari M, Ansari-Pour N. Why, When and How to Adjust Your P Values? Cell J. 2019;20(4):604–7.

132. Huang DW, Sherman BT, Lempicki RA. Systematic and integrative analysis of large gene lists using DAVID bioinformatics resources. Nat Protoc. 2009;4(1):44–57.

133. Huang DW, Sherman BT, Lempicki RA. Bioinformatics enrichment tools: paths toward the comprehensive functional analysis of large gene lists. Nucleic Acids Res. 2009 Jan;37(1):1–13.

Supplemental figures and tables

Figure S1. Hierarchical cluster analysis of samples based on Aitchison distances calculated using transcript profiles. Outliers shown in red. These were removed for subsequent analyses.

Figure S2. Principal Components Analysis based on Aitchison distances calculated using transcript profiles. Samples grouped by genotype and [CO_2].

Table S1. List of transcript identifiers having effect sizes greater than $\pm$ 1. Transcripts are sorted by increase or decrease from the control, which is either the Control Genotype (CG) for between species comparisons or 380 ppm [CO_2] for within species comparisons. *(Included as separate tab delimited (.txt) file.)*

Table S2. Full functional annotation tables (outputs from DAVID) for each treatment group stored as .txt files. Table S2a provides is an expanded version of Table 2 in the main text including all Functional Annotation Clusters with Enrichment Scores greater than 1.3. *(All files are included as separate tab delimited (.txt) files.)*

Table S3. ANOVA results of within genotype comparisons of the effect of [CO_2], incorporating dataset, GCMS or NMR, as a covariate.

Table S4. Flowering genes assessed for effect size in within genotype comparisons of the effect of [CO_2]. Whether genes were present in transcript dataset is indicated. *(Included as separate tab delimited (.txt) file.)*

Table S5. Hoagland's Solution.

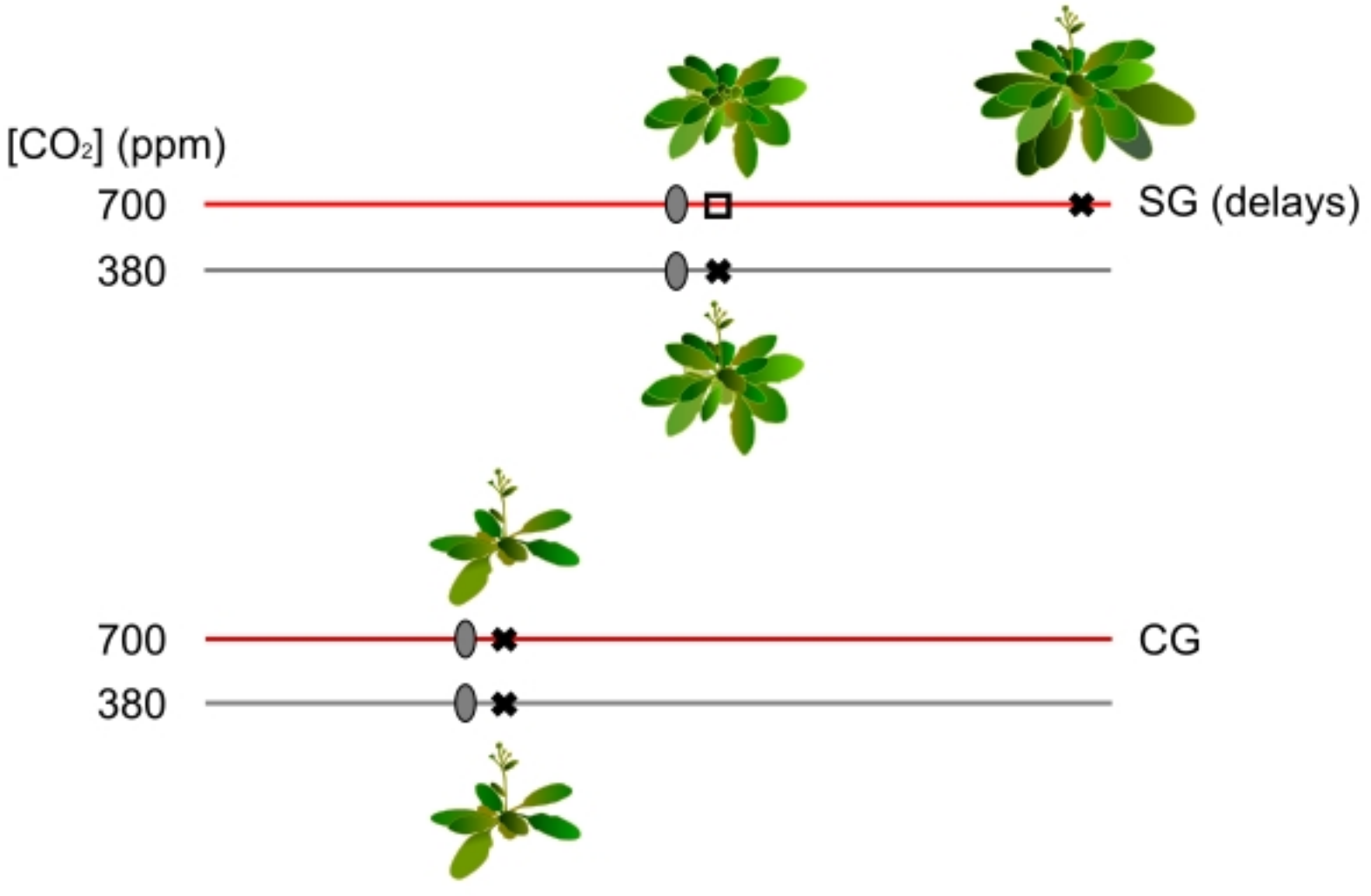
[CO2] (ppm)
700
380
SG (delays)
700
380
CG
Reproductive bolt visible
Timepoint at analogous leaf number at bolt at 380 ppm
Harvest timepoint

Figure

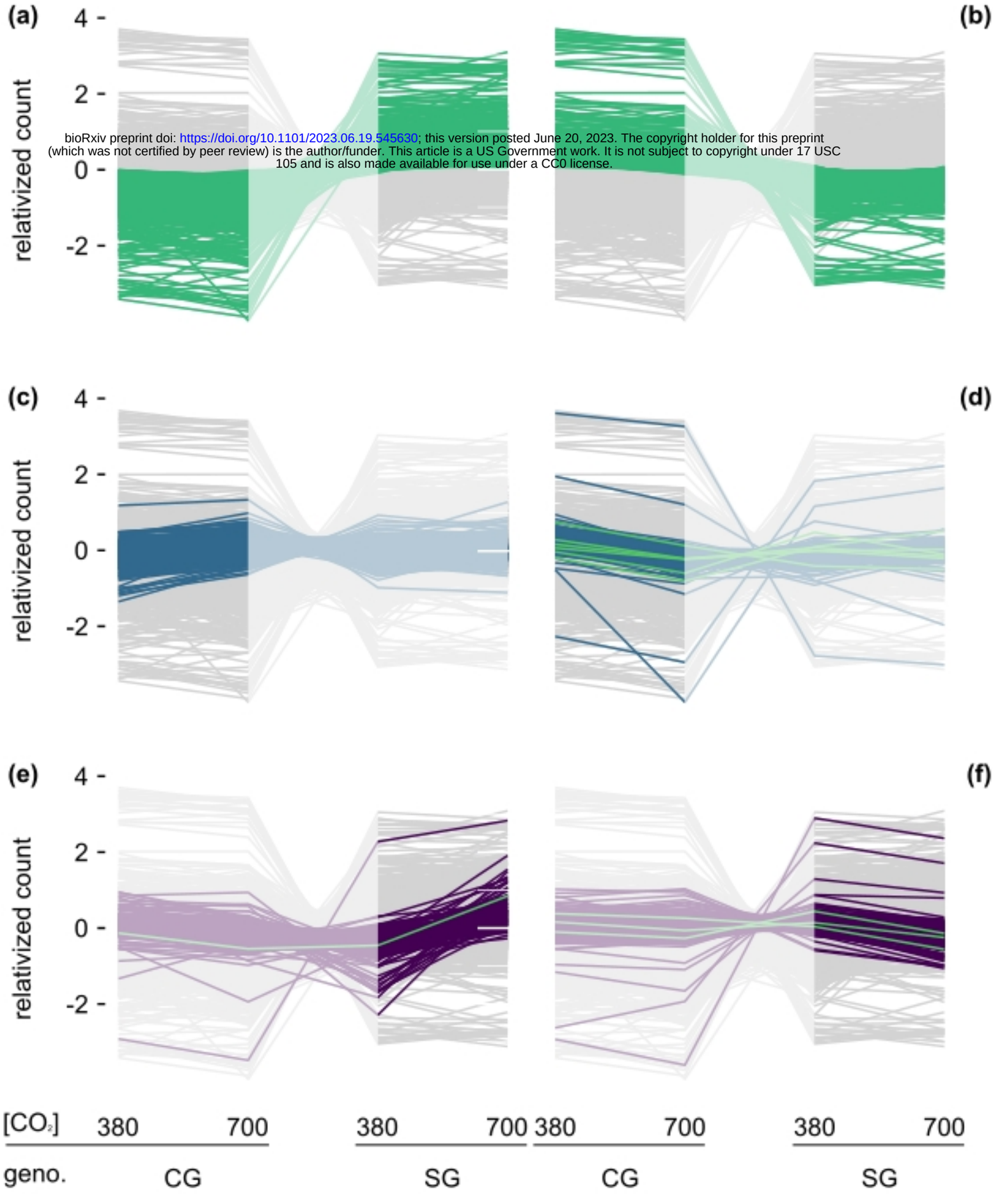

Figure

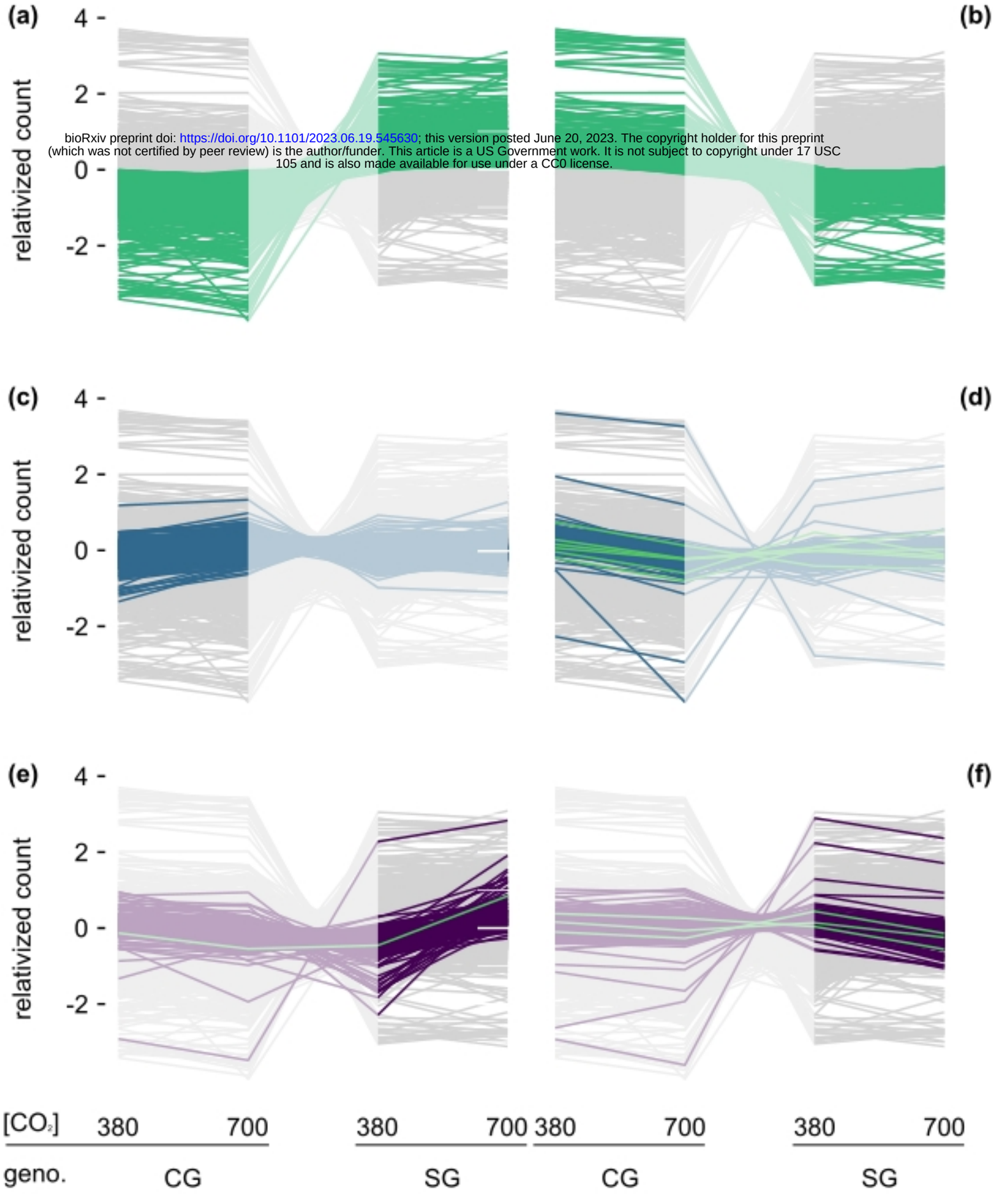

Figure

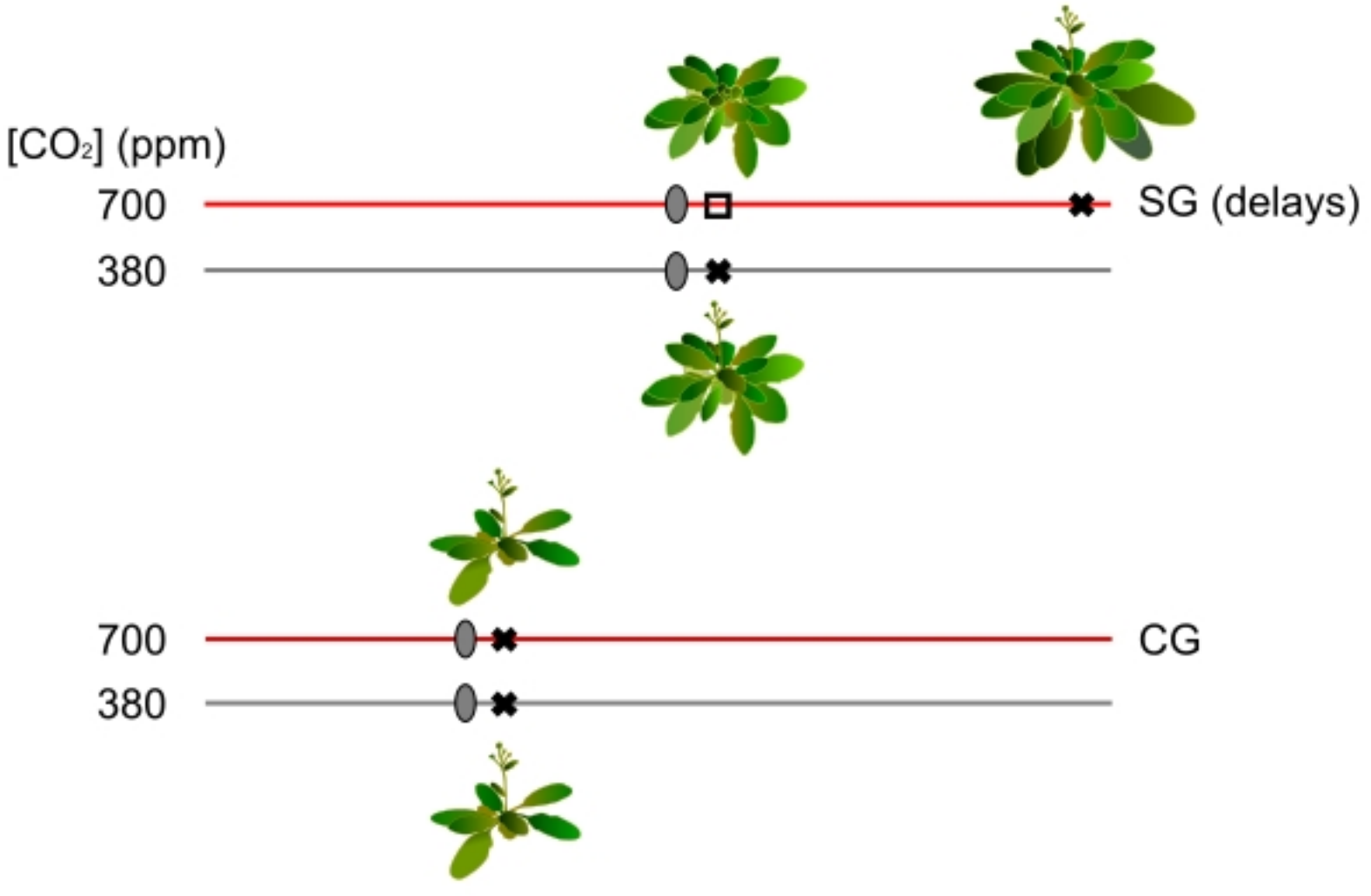
[CO2] (ppm)
700
380
SG (delays)
700
380
CG
Reproductive bolt visible
Timepoint at analogous leaf number at bolt at 380 ppm
Harvest timepoint

Figure